

## A STUDY OF EDGE-ON GALAXIES WITH THE HUBBLE SPACE TELESCOPE'S ADVANCED CAMERA FOR SURVEYS. II. VERTICAL DISTRIBUTION OF THE RESOLVED STELLAR POPULATION

ANIL C. SETH  
University of Washington

JULIANNE J. DALCANTON\*  
University of Washington

ROELOF S. DE JONG  
Space Telescope Science Institute  
*Accepted by the Astronomical Journal, June 4, 2005.*

### ABSTRACT

We analyze the vertical distribution of the resolved stellar populations in six low-mass ( $V_{\max} = 67 - 131 \text{ km s}^{-1}$ ), edge-on, spiral galaxies observed with the Hubble Space Telescope Advanced Camera for Surveys. In each galaxy we find evidence for an extraplanar stellar component extending up to 15 scale heights (3.5 kpc) above the plane, with a scale height typically twice that of 2-D fits to  $K_s$  band 2MASS images. We analyze the vertical distribution as a function of stellar age by tracking changes in the color-magnitude diagram. The young stellar component ( $\lesssim 10^8$  yrs) is found to have a scale height larger than the young component in the Milky Way, suggesting that stars in these low mass galaxies form in a thicker disk. We also find that the scale height of a stellar population increases with age, with young main sequence stars, intermediate age asymptotic giant branch stars, and old red giant branch stars having successively larger scale heights in each galaxy. This systematic trend indicates that disk heating must play some role in producing the extraplanar stars. We constrain the rate of disk heating using the observed trend between scale height and stellar age, and find that the observed heating rates are dramatically smaller than in the Milky Way. The color distributions of the red giant branch stars well above the midplane indicate that the extended stellar components we see are moderately metal-poor, with peak metallicities around  $[\text{Fe}/\text{H}] = -1$  and with little or no metallicity gradient with height. The lack of metallicity gradient can be explained if a majority of extraplanar RGB stars were formed at early times and are not dominated by a younger heated population. Our observations suggest that, like the Milky Way, low-mass disk galaxies also have multiple stellar components. In its structure, mean metallicity and old age, the RGB component in these galaxies seems analagous to the Milky Way thick disk. However, without additional kinematic & abundance measurements, this association is only circumstantial, particularly in light of the clear existence of some disk heating at intermediate ages. Finally, we find that the vertical dust distribution has a scale height somewhat larger than that of the main sequence stars.

*Subject headings:* galaxies:spiral – galaxies:structure – galaxies:formation – galaxies:individual(IC 5052, NGC 55, NGC 4144, NGC 4244, NGC 4631, NGC 5023) – dust

### 1. INTRODUCTION

Galactic structure has long been recognized as a key constraint on theories of galaxy formation. The presence of two distinct components – disks and spheroids – suggests that at least two separate physical mechanisms were active during the formation of spiral galaxies. Within the Milky Way, however, detailed analyses of the kinematics and chemistry of nearby stars have revealed additional components: a thin disk with scale heights dependent on age, a thick disk and a stellar halo. Each of these components place unique constraints on the Galaxy's evolution. In particular, the ages and metallicities of the old thin disk, thick disk and halo indicate that they are remnants of the initial stages in the assembly of the galaxy and

thus constrain the early evolution of galaxies.

Several scenarios for the creation of the old thin and thick disks are consistent with current observations in the Milky Way. These scenarios can be categorized into three main types: (1) the creation of a thick disk from a thin disk by heating by molecular clouds, spiral arms, star formation or accretion events (e.g. Spitzer & Schwarzschild 1951; Barbanis & Woltjer 1967; Lacey 1991; Kroupa 2002; Quinn et al. 1993; Gnedin 2003). (2) the slow collapse of the proto-Galaxy forming the thick and thin disk in succession (e.g. Eggen et al. 1962; Gilmore 1984), and (3) the formation of a thick disk from mergers, either by direct accretion of stars or by *in situ* formation from accreted gas (e.g. Bekki & Chiba 2001; Gilmore et al. 2002; Abadi et al. 2003; Brook et al. 2004). In this last scenario the thin disk would likely form by a settling of gas from the merger events. It is widely assumed that the stellar halo forms from accreted satellites (see review

Electronic address: seth@astro.washington.edu  
\*Alfred P. Sloan Research Fellow  
Electronic address: jd@astro.washington.edu  
Electronic address: dejong@stsci.edu

by Freeman & Bland-Hawthorn 2002). Determination of which processes are important in galaxy formation requires the study of stellar components in other galaxies.

Unfortunately, detailed analyses of older stellar components are difficult outside the Milky Way. Some thick disks and stellar halos have been identified using broadband surface photometry (e.g. Burstein 1979; Tsikoudi 1979; Dalcanton & Bernstein 2002; Pohlen et al. 2004; Zibetti et al. 2004), but their low surface brightness precludes all but a most cursory study of their structure and stellar content. Recently, HST imaging has begun to allow richer analyses of the resolved stars in the thick disk and halo (Brown et al. 2003; Tikhonov et al. 2005; Mould 2005). The resulting color-magnitude diagrams can provide robust constraints on the metallicities and ages of the stars which dominate these old components in other galaxies.

In this paper we take advantage of a large database of ACS imaging of nearby edge-on galaxies to analyze the stellar populations of the galaxies as a function of height above the galaxy midplane (“disk height”). The wide field of view of ACS allows us to track changes in the color-magnitude diagram to more than 3 kpc above the plane. Moreover, our sample galaxies have much lower masses than the Milky Way, and thus constrain how the extraplanar stellar content varies with galaxy mass. The properties of the sample and their global color-magnitude diagrams are given in Seth et al. (2005) (Paper I). In this paper, we study the spatially resolved stellar populations in eight fields of six galaxies that were close enough to determine accurate Tip of the Red Giant Branch (TRGB) distances. In particular, we show that there is a significant stellar population high above the plane of these galaxies and that these stars are old and metal-poor, comparable to high-latitude stellar populations in the Milky Way.

In §2, we review the results of Paper I for these six galaxies and describe the completeness corrections used to correct the stellar number counts in the remainder of the paper. In §3 we show that we trace stars in the host galaxies out to many scale heights and that these stars have a larger scale height than expected from fits to 2MASS  $K_s$  band images. In §4 we select three populations of stars from color-magnitude diagrams (CMDs) and show that the scale height of a stellar population increases with age. We derive metallicity distribution functions for the extended stellar component in §5 and then conclude by discussing our results in a broader context in §6.

## 2. REVIEW OF THE GALAXY PROPERTIES

Table 1 shows the position, type, maximum circular velocity ( $V_{\max}$ ), distance modulus ( $m - M_{\text{TRGB}}$ ), scale length ( $h_r$ ) and the  $K_s$  band half-light height ( $z_{1/2}$ ) of the six galaxies we will discuss in this paper. The latter two parameters were determined from 2-D model fits to 2MASS  $K_s$  band data, presented in Paper I. The vertical component of these models is defined using the distribution of an isothermal population of stars (van der Kruit & Searle 1981):

$$\Sigma(z) \propto \text{sech}^2\left(\frac{z}{z_0}\right) \quad (1)$$

where  $\Sigma(z)$  is the surface brightness or density at a position  $z$  above the midplane, and  $z_0$  is the scale height. We will use this functional form to fit vertical distributions throughout this paper. Note, however, that this is one of many equations commonly used to describe the vertical distribution of stars in galaxies, a good overview of which can be found in (Pohlen et al. 2000). Most of these functional forms vary near the midplane, but have similar exponential declines at large disk heights. When comparing galaxies in this paper, the disk heights will be normalized by the  $z_{1/2}$  parameter, which gives the height containing 50% of the  $K_s$  band light in the model fits. It is related to  $z_0$ ,  $z_{1/2} = 0.549 z_0$ , and is similar to the exponential scale height  $h_z$ , which at large scale heights is equal to  $\frac{1}{2}z_0$  (van der Kruit & Searle 1981). The values of  $z_{1/2}$  for the six galaxies range from 160–280 pc. For comparison, the Milky Way thin disk has exponential scale heights ranging from  $\sim 100$  pc at young ages (Schmidt 1963) to 330 pc (Chen et al. 2001) at older ages.

All six galaxies are within 8 Mpc and are type Sc or later. The maximum circular velocities are all below 135 km/sec suggesting that these objects are closer in mass to the LMC than to the Milky Way. We note that all the galaxies except NGC 4631 have circular velocities well below 120 km/sec, which appears to mark a break in the dust properties (Dalcanton et al. 2004) and current metallicity (Garnett 2002) in spiral galaxies. The scale lengths of our sample galaxies range from 0.9 to 1.6 kpc,  $\sim 2$ -3 times smaller than the Milky Way scale length<sup>1</sup>. None of the galaxies has an apparent bulge component, although NGC 4244 does have a prominent central stellar cluster, which is clearly visible in the ACS and 2MASS  $K_s$  band images.

Our observations include eight HST/ACS fields in the six galaxies shown in Table 1 and are described fully in Paper I (Seth et al. 2005). These observations were obtained to study the dust-lane properties of these galaxies, and hence are centered on the galaxy midplane. The dimensions of these eight fields are given in Table 2, which shows the minimum and maximum disk radius in terms of the scale length and the minimum and maximum disk height in terms of  $z_{1/2}$ . In general, each field is located close to the center of the galaxy. However, two of the galaxies, NGC 55 and NGC 4631 have additional fields located further out in the disk that are given a ‘-DISK’ suffix. Note that many of the galaxies lie diagonally across the chip meaning that the extremities of the ranges given in Table 2 are not well sampled. In this paper, we focus on the vertical distributions of the stars, and where not otherwise noted, analyze all data at the same disk height together.

The approach proposed above is valid as long as the scale height of disk components does not vary substantially with radius, an assumption that has been verified through observations of edge-on galaxies (e.g. van der Kruit & Searle 1981; Pohlen et al. 2004). We note however, that there are some analyses which indicate that the scale height of galaxies

<sup>1</sup> The Milky Way thin & thick disk scale lengths are rather uncertain with recent values ranging between 2-4 kpc (e.g. Ng et al. 1996; Mendez & van Altena 1998; Ojha 2001), we will use a scale length of 3 kpc for comparisons to the Milky Way made in this work.

TABLE 1  
GALAXY SAMPLE PROPERTIES

Galaxy	RA(J2000)	Dec(J2000)	<i>incl.</i>	Type	$V_{max}$ km/sec	$m - M_{TRGB}$	$h_R$ [ $''$ ]	$h_R$ [kpc]	$z_{1/2}$ [ $''$ ]	$z_{1/2}$ [pc]
IC 5052	20 52 02.9	-69 11 45	89	SBcd	79	28.90	53.87	1.57	7.33	214
NGC 55	00 14 54.4	-39 11 59	80	SBm	67	26.63	93.30	0.96	23.34	240
NGC 4144	12 09 58.3	+46 27 28	83	SBc	67	29.36	30.56	1.10	6.96	251
NGC 4244	12 17 29.5	+37 48 28	84.5	Sc	93	28.20	84.27	1.78	12.15	257
NGC 4631	12 42 07.7	+32 32 33	85	SBcd	131	29.42	35.49	1.32	7.54	280
NGC 5023	13 12 11.7	+44 02 17	88	Sc	77	29.10	39.81	1.28	5.10	160

NOTE. — RA, Dec, TRGB distance moduli,  $h_r$ , and  $z_{1/2}$  taken from Paper I. Galaxy Types and  $V_{max}$  from HYPERLEDA/LEDA (Paturel et al. 1995, 2003). Inclinations taken from Becker et al. (1988); Hummel et al. (1986); Martin (1998); Olling (1996); Hummel & Dettmar (1990); de Grijs & van der Kruit (1996) (in same order as table).

TABLE 2  
FIELD PROPERTIES

Field	# Stars	$R_{min}$ [R/ $h_r$ ]	$R_{max}$ [R/ $h_r$ ]	$z_{min}$ [ $z/z_{1/2}$ ]	$z_{max}$ [ $z/z_{1/2}$ ]
IC 5052	68636	-2.9	1.9	-22.1	15.6
NGC 55	281536	-1.6	1.4	-5.8	5.3
NGC 55-DISK	253108	3.3	6.2	-7.3	5.5
NGC 4144	60552	-2.3	5.9	-18.7	14.6
NGC 4244	121238	-1.4	1.2	-6.8	10.5
NGC 4631	104940	-3.1	3.4	-17.8	10.2
NGC 4631-DISK	97656	-10.1	-1.6	-21.2	14.8
NGC 5023	42293	-2.7	3.1	-18.1	25.3

flares with increasing radius, both in our own Galaxy (López-Corredoira et al. 2002) and in edge-on galaxies (de Grijs & Peletier 1997; Narayan & Jog 2002). However, de Grijs & Peletier (1997) show that in their sample of edge-on galaxies, late-type galaxies such as those observed here have little or no flaring. In one of our galaxies, NGC 4244, flaring of the HI gas by a factor of  $\sim 3$  is seen between radii of 8-13 kpc (Olling 1996). Even if similar flaring occurs in the stellar distribution, the star counts at the disk heights we consider here will still be dominated by stars located (radially) near the center of the galaxy. We note that we do see some evidence for modest flaring in our two ‘-DISK’ fields which lie at large radii (see §4.2.1).

In Paper I we presented the color-magnitude diagrams (CMDs) for each of the galaxy fields discussed here. These are reproduced in Figure 1 which shows the F606W-F814W color vs. the F814W magnitude. All magnitudes in this paper are given in the VEGA-mag system (see Paper I for details). Each of the CMDs show plumes at F606W-F814W colors of  $\sim 0.1$  and  $\sim 1.3$  which are young main sequence (MS) and helium burning (HeB) stars respectively. An old RGB can be seen in each galaxy at colors of  $\sim 1$  and an intermediate-age asymptotic giant branch (AGB) extends from the tip of the RGB to redder colors. Further details on the components can be found in §4.1 and in Paper I. The boxes shown in Figure 1 isolating these components will be discussed in greater detail in §4.

### 2.1. Completeness Corrections

As described in Paper I, we conducted extensive artificial star tests to characterize the completeness in each field as a function of magnitude, color and location. The galaxies in our sample have high surface brightnesses near their midplane making the completeness there much lower (see Fig. 2 from Paper I). The goal of this paper is to analyze the vertical distribution of stellar populations, and therefore correcting for this varying completeness is critical.

For each field, over 5 million artificial stars were inserted at random positions, with magnitudes between F606W of 18 and 29, and with F606W-F814W colors between -1 and 3. These stars were then run through the same pipeline used to determine the stellar photometry. Artificial stars that coincided with actual sources were considered detected only if the input magnitude of the artificial star was brighter than the actual source in both bands.

To enable completeness corrections for individual stars, we determined our completeness for the artificial stars in bins of magnitude, color and local surface brightness. For the magnitude and color, we used 0.15 magnitude wide bins. At its steepest, the completeness as a function of magnitude varies by at most 6% over 0.15 magnitudes, so any error introduced by the binning should be smaller than that. We then determined the size of the surface brightness bins such that there would be  $\sim 50$  stars in each final bin. Determining the completeness from 50 stars gives a random error in the completeness of  $\sim 6\%$ . An aperture around each star from 11 to 14 pixels was used to determine the local surface brightness. We determined the surface brightness level from the F606W image so as to include the effects of the HII region emission visible in a number of galaxies (most notably NGC 55, which therefore has the brightest completeness level in Fig. 2). This emission is not seen at all in the F814W images, due to the lack of strong emission lines in F814W bandpass. Using this binned completeness function, we are able to determine the completeness of any individual star based on its color, magnitude and local surface brightness level to within  $\sim 10\%$ . In the stellar density profiles presented in §3 & §4, the completeness corrections are up to 200% near the midplane, but fall to  $\lesssim 30\%$  at  $z/z_{1/2} > 3$ .

In addition to correcting for the completeness, magnitude limits must also be set to insure that we are not using stars fainter than we can detect in the higher surface

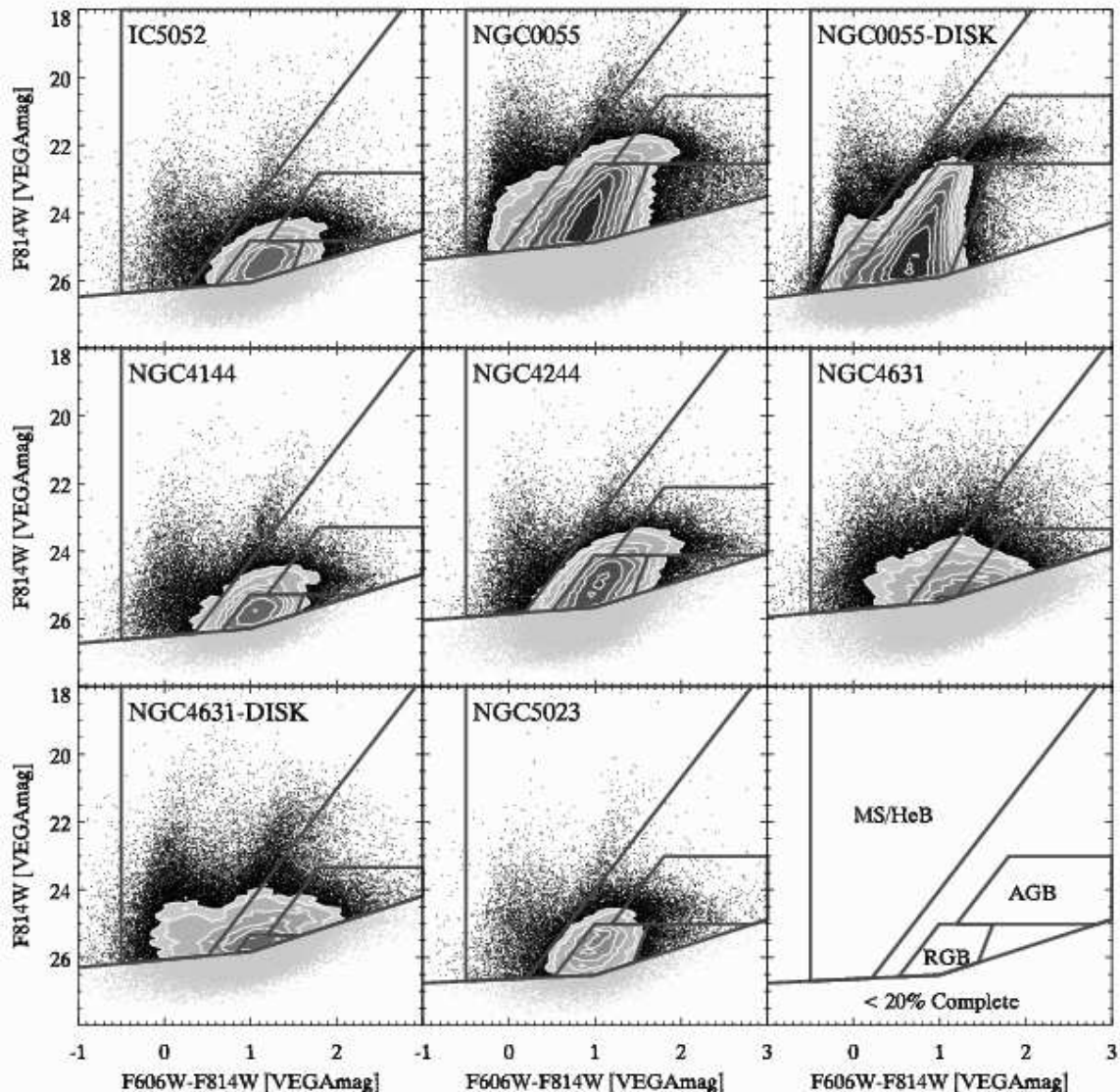


FIG. 1.— Color-magnitude diagrams of each galaxy. Contours are used where the density of points becomes high. The contours are drawn at densities of 75, 100, 150, 200, 250, 350, 500, 750, 1000, and 1500 stars per 0.1 magnitude and color bin. The bottom-left panel contains a key to the gray lines which demarcate sections of the CMD. The line across the bottom shows the 20% completeness limit in bright regions of the galaxy (see §2.1 for details) and the other lines show the regions used in each galaxy for the MS/HeB, AGB and RGB stars.

brightness regions of the image (i.e. the midplane). We therefore choose to limit our analysis to regions of the CMD that fall above a conservative 20% completeness limit in regions of high surface brightness. Figure 2 shows the 20% completeness limits for the brightest regions in each field. As can be seen, the completeness limit rises towards redder colors, and steepens at colors redder than  $F606W-F814W$  of 1. To make a smooth boundary that is easily applied to our data, we fit the 20% completeness curves to two lines intersecting at  $F606W-F814W=1$ . Table 2 shows the results of these fits, by giving the completeness limit at  $F606W-F814W$  of -1 ( $F814W_{\text{lim},-1}$ ), 1 ( $F814W_{\text{lim},1}$ ), and 3 ( $F814W_{\text{lim},3}$ ). We use these limits throughout this paper to insure that comparisons made between stellar populations at different disk heights are valid.

We note here that although we can correct for incom-

pleteness due to crowding, we cannot correct for the attenuation of stars by dust. We will show in §4 that all the galaxies in our sample are optically thick near their midplanes. Therefore at low galactic latitudes, our completeness corrected stellar census will fall short of the true number of stars.

### 3. VERTICAL DISTRIBUTION OF STARS

We demonstrate in this section that there are significant numbers of stars well above the planes of all our disks and that the profiles of these stars do not fit the profiles expected from the ground-based  $K_s$  band galaxy fits.

In Figure 3 we present the completeness corrected surface density profiles of all the detected stars ( $\Sigma_{\text{all}}$ ) above the completeness limits given in Table 3. Two lines are shown for each galaxy, giving the profile on both sides

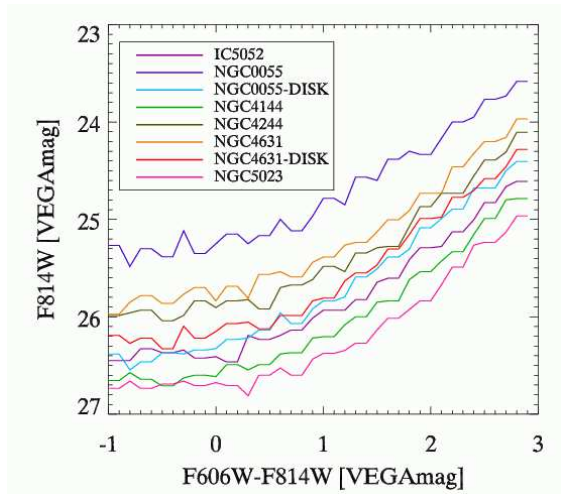


FIG. 2.— The 20% completeness limit in the brightest sections of each field as a function of color. The variation from field-to-field is due to increased crowding / higher surface brightness regions in some fields.

TABLE 3  
20% COMPLETENESS LIMITS

Field	$F814W_{\text{lim},-1}$ [mag.]	$F814W_{\text{lim},1}$ [mag.]	$F814W_{\text{lim},3}$ [mag.]
IC 5052	26.48	26.05	24.51
NGC 55	25.39	24.86	23.51
NGC 55-DISK	26.52	25.89	24.28
NGC 4144	26.72	26.28	24.67
NGC 4244	26.04	25.65	24.07
NGC 4631	25.94	25.49	23.88
NGC 4631-DISK	26.30	25.83	24.18
NGC 5023	26.76	26.52	24.88

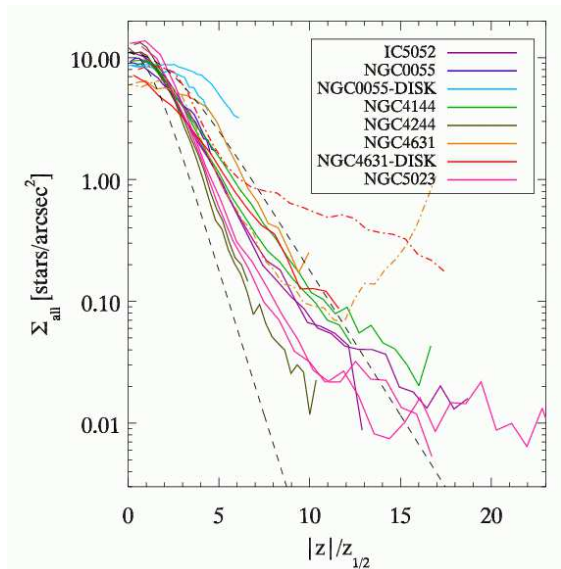


FIG. 3.— The surface density of stars as a function of height from the midplane. Curves have been completeness corrected as described in the text. Each galaxy has two lines, one for above and below the plane. The dashed lines indicate stellar distributions with scale heights 1 & 2  $\times$  that of the  $K_s$  band fits to the disks. The dot-dashed lines for the NGC 4631 fields indicate the regions where contamination of stars from companion NGC 4627 is significant.

of the disk. To determine the surface density, stars were binned as a function of scale height. After binning, the completeness-corrected number of stars was divided by the area of the bin to obtain the surface density. Only bins with an area of more than 300 arcsec<sup>2</sup> are plotted.

Figure 3 shows that we trace the stellar component of each galaxy out to large disk heights, with several galaxies being traced beyond  $10z_{1/2}$ . The profiles in general are fairly symmetric, the most notable exception being NGC 4631 and NGC 4631-DISK. These fields are contaminated on one side (shown using dot-dashed lines) by the presence of the companion galaxy NGC 4627 (see Fig. 3 from Paper I). The decrease of the profiles with increasing scale height out to the edge of the fields strongly suggests that the profiles remain above the surface density of foreground Galactic stars and background unresolved dwarf galaxies in our magnitude range. Only above  $10z_{1/2}$  in IC 5052 and NGC 5023 is there some evidence for the leveling off that would be expected as we reach the foreground/background level. Note that the galaxies are all at galactic latitudes above  $35^\circ$ . We therefore can safely assume that a vast majority of stars in our images are located in the host galaxies and we make no corrections for foreground/background sources.

The dashed lines in Figure 3 show  $\text{sech}^2$  profiles with scale heights one and two times the measured  $K_s$  band scale height (note that because the plot is scaled by the  $K_s$  band scale height these profiles are the same for each galaxy). As described in detail in Paper I, models were fit using a Levenberg-Marquardt algorithm with uniform weighting on all unmasked pixels to  $K_s$  band 2MASS data. Because the 2MASS surface photometry has a limiting isophote of  $K_s \sim 20.0$  mag/arcsec<sup>2</sup>, only relatively high surface brightness features could be fit. The typical  $K_s$  band peak surface brightness of our galaxies is  $\sim 18$  (Paper I, Table 2), which means that galaxies are only detected in the  $K_s$  images out to a few  $z_{1/2}$  from the midplane. Although the  $K_s$  band light is often thought to be dominated by the RGB stars that trace an old stellar population, we will show in §4 that in these low mass, late-type galaxies, it more closely traces the young and intermediate age populations and is thus dominated by red supergiant and AGB stars.

Figure 3 shows that the outer portions of the stellar density profiles of the galaxies appear to be broader than indicated by the  $K_s$  band scale height. To quantify this, we fit the stellar density profiles between  $5z_{1/2}$  and  $10z_{1/2}$  on each side of the midplane in each galaxy. Only profiles with data beyond  $8z_{1/2}$  were fit (thus excluding NGC 55, NGC 55-DISK and one side of NGC 4244). In the Milky Way, the stellar profile deviates from the thin disk profile beyond  $\sim 1$  kpc above the plane (Gilmore & Reid 1983). For our galaxies,  $5z_{1/2}$  is  $\sim 1$  kpc. Therefore we would expect our fitting range to be sensitive to a possible thick disk component in these galaxies. The scale heights of these fits above and below the midplane are shown in the third and fourth columns (respectively) of Table 4. All of the fitted stellar profiles are significantly broader ( $\times 1.5$ - $2.4$ ) than the  $K_s$  band scale height. This observation strongly suggests that these galaxies contain a more broadly distributed stellar component not traced by the  $K_s$  band 2MASS images.

We note that the fitted scale heights, both in the  $K_s$

TABLE 4  
RESOLVED STELLAR COMPONENT SCALE HEIGHTS

Field	$K_s$ $z_0$ [pc]	All + $z_0$ [pc]	All - $z_0$ [pc]	MS $z_0$ [pc]	AGB $z_0$ [pc]	RGB $z_0$ [pc]	$h_r/z_{0,MS}$	$h_r/z_{0,AGB}$	$h_r/z_{0,RGB}$
IC 5052 <sup>a</sup>	390	767±30	686±44	261±11	467±6	655±6	6.0	3.4	2.4
NGC 55	437			327±24	644±10	701±3	2.9	1.5	1.4
NGC 55-DISK	437			526±1	741±15	999±6	1.8	1.3	1.0
NGC 4144	457	940±41	965±15	374±27	699±16	934±18	2.9	1.6	1.2
NGC 4244	468	740±40		325±20	443±24	551±9	5.5	4.0	3.2
NGC 4631 <sup>b</sup>	510	927±46		510±26	895±51	1154±194	2.6	1.5	1.1
NGC 4631-DISK <sup>b</sup>	510	1131±50		505±22	1200±1	1387±73	2.6	1.5	1.0
NGC 5023 <sup>a</sup>	291	505±32	534±26	204±6	289±6	391±4	6.3	4.4	3.3

NOTE. — (a) In IC 5052 and NGC 5023, MS, AGB and RGB fits excluded disk heights below  $1.5z_{1/2}$ . All other galaxies excluded below  $3z_{1/2}$ . (b) Negative values of  $z$  excluded beyond 2 kpc due to the presence of companion galaxy NGC 4627.

band and using stellar density profiles, can differ from the true scale height due to a number of factors. First, dust attenuation can obscure light near the midplane of the galaxy. In the  $K_s$  band this attenuation should be small, and we ameliorate this problem in the fits presented here by avoiding the midplane. Second, the galaxies may not be perfectly edge-on. Based on previous observations, the least inclined of the galaxies is NGC 55, which has a  $\sim 80^\circ$  inclination (Hummel et al. 1986). This would give a fitted scale height  $\sim 30\%$  greater than the intrinsic disk scale height. We also note that NGC 55 and NGC 4631 are fairly irregularly shaped making the fits to these galaxies less reliable than for the other four galaxies.

#### 4. VARIATION IN DISTRIBUTION WITH STELLAR POPULATION

We now turn our analysis to stars selected in regions of our CMDs that isolate stellar populations with different ages. Using this method we show that the older stellar populations have an increasing scale height. In §4.3, we examine the variation of scale height in the context of disk heating models. We then present simplistic dust models in §4.4 and show that the dust extinction in these galaxies is distributed in a component that is broader than the young stellar populations.

##### 4.1. Selection of CMD regions

We attempt to separate our data into young, intermediate, and old stellar populations by selecting stars from different regions in the CMD. The young stars are found in the Main Sequence (MS) component and in the red and blue Helium Burning (RHeB, BHeB) sequences (see Paper I, Fig. 1 for a schematic CMD), all of which should contain stars under a few 100 Myr in age. For the intermediate age stars we select AGB stars brighter than and redward of the RGB, resulting in ages ranging between a few 100 Myr and a few Gyr. Lastly, for the old population of stars we select RGB stars, which have ages in excess of 1 Gyr, although some AGB stars will also be found in the same region.

The actual regions used for the selection are shown in the CMDs in Fig. 1. The bottom right figure is a cartoon illustrating the selection of the MS/HeB, AGB and RGB regions. The RGB region was selected using lines with slopes of 3.3 and 6.6 and F606W-F814W colors of 1.0 and

1.6 at the tip of the RGB. The MS region was defined by taking all stars redward of  $-0.5$  and blueward of a line with slope of 3.3 and a color of 0.7 at the TRGB magnitude. Finally, the AGB region isolates stars less than two magnitudes brighter than the TRGB magnitude and redwards of a line with slope of 3.3 and a color of 1.2 at the TRGB magnitude. These boundaries were combined with the TRGB magnitude given in Table 1 and the completeness limits from Table 3 to determine the final regions for each galaxy shown in Figure 1. The regions were chosen somewhat conservatively - e.g. we chose to put space between the MS/HeB section and the RGB so that there would be little overlap between the two due to dust extinction or large photometric errors at faint magnitudes. From here we will refer to the stars in these CMD boxes as the MS, AGB and RGB stellar populations.

##### 4.1.1. Synthetic CMDs

To determine the typical ages of stars detected in our CMD boxes and to facilitate quantitative comparisons between galaxies and their different stellar populations, we generated synthetic CMDs using the MATCH program (Dolphin 2002) and the IAC-STAR program<sup>2</sup> (Aparicio & Gallart 2004), using isochrones of Bertelli et al. (1994) and Girardi et al. (2000) in both cases. The synthetic stars were generated assuming a constant star formation rate (SFR) from 13 Gyr ago to the present, and a metallicity that steadily increased from  $[\text{Fe}/\text{H}] = -1.7$  to  $-0.4$  (Garnett 2002). We used slightly different IMFs in the two CMDs. For the MATCH CMD a pure Salpeter IMF ( $\alpha = 2.35$ ) is assumed between 0.1 and 120  $M_\odot$ , whereas in the IAC-STAR CMD we used the default Kroupa et al. (1993) IMF, which is steeper at the high mass end ( $\alpha = 2.70$ ).

To compare these CMDs to our observations, the synthetic stars were first transformed from Johnson V & I to VEGAMag F606W & F814W colors. We then mimicked observations of each galaxy as follows. First, each star was randomly assigned a surface brightness value based on the values of detected stars in each frame. Then, using the artificial star tests, we determined the chance

<sup>2</sup> This work has made use of the IAC-STAR Synthetic CMD computation code, IAC-STAR is supported and maintained by the computer division of the IAC.

each star was detected and a magnitude error based on the star’s initial F606W & F814W magnitudes (assuming the distance moduli shown in Table 1) and the surface brightness value. A final CMD was then made by randomly determining if each star was detected and applying the determined errors. The resulting CMDs looked qualitatively similar to our observed CMDs, with the most notable difference being an offset of the AGB stars to somewhat brighter magnitudes in both synthetic CMDs relative to the real data and a deficit of MS/HeB stars in the IAC-STAR CMDs relative to the MATCH and the real galaxy CMDs. This could indicate either that the galaxies have enhanced recent star formation or that their IMF is not as steep as the Kroupa et al. (1993) IMF on the high mass end.

Figure 4 shows the resulting age distribution of the MS, AGB, and RGB boxes in NGC 4144 using the MATCH and IAC-STAR synthetic CMDs. The age distributions for other galaxies are similar. This figure clearly demonstrates that we are separating the stars into young, intermediate-age and old populations with our chosen CMD boxes. However, the separation is not perfect. Each bin has significant overlaps with the others due to unavoidable photometric errors and to true overlap in the colors and magnitudes of stellar populations with different ages. The IAC-STAR CMDs have age distributions similar to the MATCH CMDs, but with the AGB populations weighted more towards older ages and a more significant contamination of old stars in the MS box (probably due to the relative lack of MS stars in the IAC-STAR models). Both effects likely result from the steeper IMF assumed for the Aparicio CMD. In the following sections of the paper, we use the MATCH CMD for comparisons with observations because it more closely reproduces the ratio of young MS and HeB stars relative to the number of older stars.

We note that these synthetic CMDs assume a *constant* star formation rate and thus are not useful in determining true star formation histories. However, we will be able to use them to get a sense of relative star formation histories (SFHs) as a function of scale height and to get a rough sense of the ages of the stars in our CMD regions.

#### 4.2. Stellar Density Profiles

Now we compare the surface density profiles of the MS, AGB and RGB stars to examine possible variations in stellar population with disk height. Figure 5 shows the completeness-corrected profiles as a function of disk height for each field. Each profile is derived using the same methodology as in §3, typically using  $\sim 10,000$  stars per field. The surface densities are then normalized to have  $\int \Sigma dz = 1$ . All the fields show a similar pattern. The MS (blue) stars have the narrowest distribution while the AGB (red) and RGB (orange/yellow) stars have broader distributions and typically show a dip near the midplane. Because we have corrected for incompleteness, the dip almost certainly due to dust absorption, as we demonstrate in §4.4 with a very simple model.

Figure 5 suggests that older stellar populations become more prominent with increasing disk height. We quantify this trend in Figure 6, which shows the ratios of surface densities in our different age bins. The ratios were normalized to those expected for a constant SFR using the MATCH synthetic CMDs (see §4.1.1). A ratio

of one in Fig. 6 therefore corresponds to a constant star formation rate and increasing values correspond to older stellar populations. We note that the ratio is only plotted where the signal-to-noise of the ratio is greater than 3. The small number of MS stars at large scale heights limits our ability to trace the  $\Sigma_{\text{RGB}}/\Sigma_{\text{MS}}$  and  $\Sigma_{\text{AGB}}/\Sigma_{\text{MS}}$  as high above the midplane as the profiles shown in Figures 3, 5 and 7. Also, NGC 4631 and NGC 4631-DISK are not included in Figure 6 because the high completeness limit results in very few RGB stars (see Fig. 1) and an increased contamination of AGB stars in the RGB box.

The top and middle panels of Figure 6 show that in each of the fields, RGB stars become more numerous relative to MS and AGB stars with increasing disk height. However, this trend shows an enormous variation from galaxy to galaxy. In IC 5052 the ratio  $\Sigma_{\text{RGB}}/\Sigma_{\text{MS}}$  becomes as high as  $\sim 100$  times the midplane value, while in NGC 55 and NGC 4244 the increase is much more moderate, to  $\lesssim 10$  times the midplane value. This variation is most likely the result of a range of recent SFRs in our galaxies. The ratio  $\Sigma_{\text{RGB}}/\Sigma_{\text{AGB}}$  is much more consistent from galaxy-to-galaxy, however. This may result from the overlapping time range spanned by stars in the AGB and RGB boxes and/or the large time ranges these boxes span relative to the MS. We argue in §5 that the RGB population is likely to be dominated by truly old stars much older than the AGB population. Interestingly, the field showing the the flattest  $\Sigma_{\text{RGB}}/\Sigma_{\text{AGB}}$  profile was the NGC 55-DISK field located in the outer parts of the NGC 55 disk, perhaps suggesting a different star formation or dynamical history at large radii ( $\sim 5 \times h_R$ ). However, this galaxy is the least inclined in our sample and is somewhat irregular in shape, therefore results for this one system should not be overinterpreted.

The low values of  $\Sigma_{\text{AGB}}/\Sigma_{\text{MS}}$  and the high values of  $\Sigma_{\text{RGB}}/\Sigma_{\text{AGB}}$  result from a lack of AGB stars compared to the constant SFR MATCH synthetic CMD. This would seem to suggest that the galaxies’ star formation histories (SFHs) are depressed at intermediate ages and enhanced at young ages. However, as we noted in §4.1, the AGB morphologies in the synthetic CMDs are not well matched to the observational CMDs, probably because of the difficulty in modeling the AGB phase of evolution (Marigo 2001). This discrepancy combined with the differences seen between the two sets of synthetic CMDs suggests that a derivation of accurate SFHs using just the brightest stars in a galaxy is not yet possible.

To check if the scatter in the  $\Sigma_{\text{RGB}}/\Sigma_{\text{MS}}$  ratio was in part due to varying radial coverages of the galaxies (Table 3), we remade the plots in Figure 6 using only stars within the central scale length of each galaxy. These plots were similar to those shown and showed comparable scatter. This suggests that the observed variations from galaxy to galaxy in the stellar populations ratio reflect global differences in the galaxies’ SFHs and/or vertical structure. For instance, if we assume the trend towards older populations with increasing scale height results from disk heating, then the scatter in Figure 6 suggests substantial variations between galaxies in either the mechanisms that heated the disk, or the SFH of the disk. Despite these variations, Figure 6 gives strong evidence that overall the age of the stellar populations increases

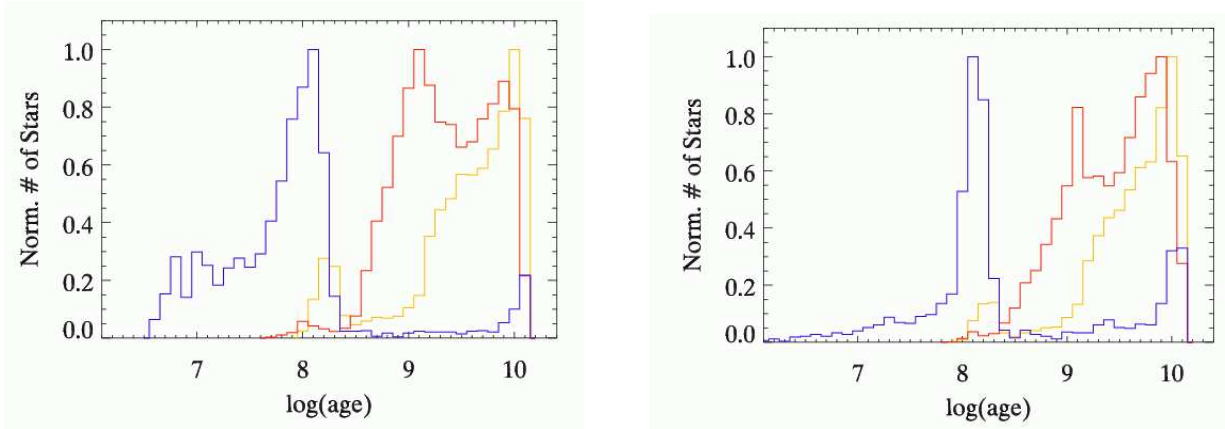


FIG. 4.— Histogram of ages detected in defined CMD boxes (see Fig. 1) for NGC 4144 assuming a constant star formation rate from 13 Gyr to the present. Histograms are based on synthesized CMDs created with the MATCH (left) and IAC-STAR (right) programs as described in §4.1. These plot shows that stars in the MS box (blue) are dominated by stars  $\sim 100$  Myr in age, while the AGB (red) and RGB (orange/yellow) boxes have typical ages of  $\sim 1$  Gyr and  $\sim 10$  Gyr respectively. Similar plots for other galaxies are qualitatively similar.

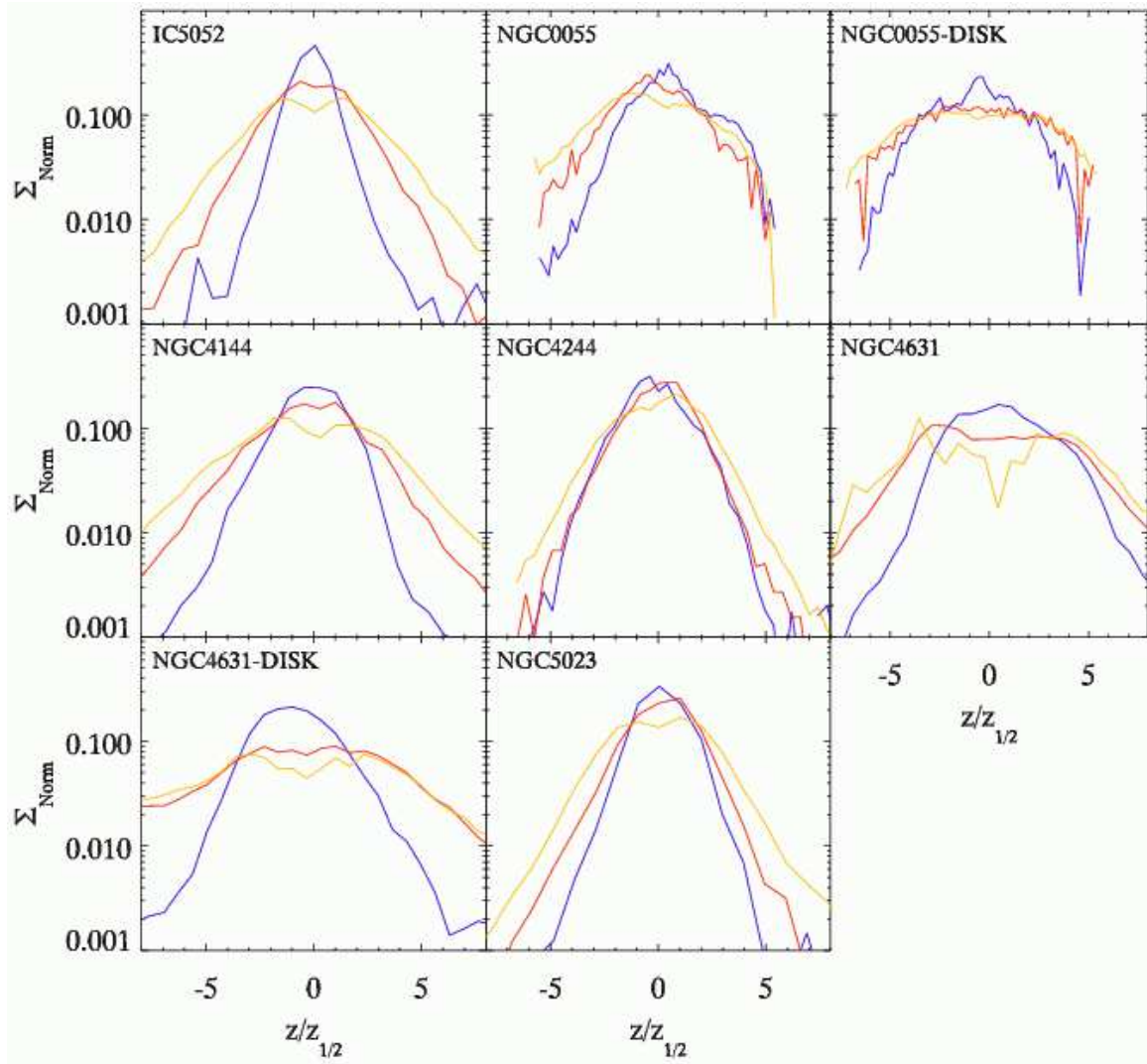


FIG. 5.— The normalized surface density as a function of scaleheight for young MS (blue), intermediate-age AGB (red) and old RGB (orange/yellow) stars. Each surface density distribution was normalized to integrate to one. Note that in all cases the MS distribution is the most peaked while the RGB distribution is the widest.



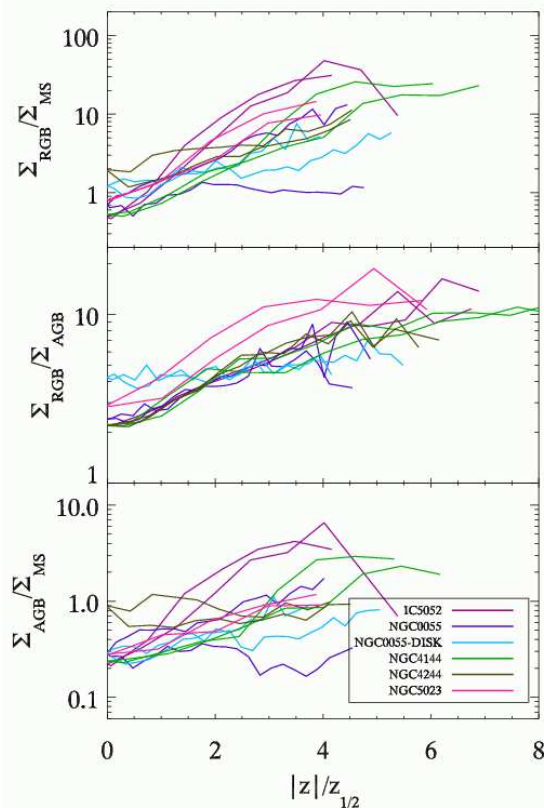


FIG. 6.— The ratio of the surface density of different stellar populations as a function of disk height: RGB/MS (top), RGB/AGB (middle), and AGB/MS (bottom). Points were normalized based on the number counts of a constant star formation rate model, e.g. a value of 1 suggests a constant star formation rate, while values  $>1$  suggest a decrease in the star formation rate with time. Note that the MATCH synthetic CMDs were used in this normalization (§4.1.1). Only points with a signal-to-noise  $> 3$  are plotted. The plots clearly show that the stellar populations become older with increasing disk height.

with increasing scale height.

#### 4.2.1. Stellar Population Scale Heights

To further quantify the differences in the vertical distribution of the three CMD regions, we fit each surface density profile to a  $\text{sech}^2$  function in which the normalization, central position, scale height ( $z_0$ ), and background level were all allowed to vary. We fit each profile only at disk heights  $>3z_{1/2}$  to avoid the dips near the midplane, except in IC 5052 and NGC 5023 where we used disk heights  $>1.5z_{1/2}$  to allow fitting of the very narrow  $\Sigma_{\text{MS}}$  profiles. Figure 7 shows the resulting fits to the  $\Sigma_{\text{MS}}$ ,  $\Sigma_{\text{AGB}}$ , and  $\Sigma_{\text{RGB}}$  profile of each galaxy, in the top, middle and bottom panels respectively. The observed profiles are shown as a solid line, while the best fitting  $\text{sech}^2$  function is shown as a dashed line. The dotted lines at  $\pm 3z_{1/2}$  ( $\pm 1.5z_{1/2}$  in IC 5052 and NGC 5023) delineate the region excluded from the fit. The error bars on the data points are used to weight the  $\text{sech}^2$  fits and reflect Poisson errors in the number counts, but do not include uncertainties in the completeness corrections. The scale height of the best-fitting  $\text{sech}^2$  function is shown in the upper-left corner of each panel, and the error shown is scaled by the square root of the reduced  $\chi^2$  of the fit. The

reduced  $\chi^2$  values for a majority of the fits were between 0.8 and 1.3, but were larger for NGC 55 and NGC 4631 due to their irregular structure. Scale heights and errors for all the fits are shown in Table 4.

We find that in each galaxy, the MS scale height value is the narrowest followed by the AGB and then the RGB. In all cases the RGB population is significantly broader than the AGB, MS and  $K_s$  band  $z_0$  values. This result strongly suggests the presence of an older component with larger scale height. An analysis of the variations in scale height of the MS, AGB and RGB populations with scale length in each of the galaxies turned up no obvious trends. We also identified no trends with galaxy rotation speed, due to the small range of masses spanned by our sample galaxies. We note that in some cases, the  $z_0$  derived for all stars (§3) is somewhat larger than the  $z_0$  derived for just the RGB stars. This results from the lower scale heights used in the fits to the different stellar populations - if the lower limit for the fit to all stars is reduced from  $5z_{1/2}$  to  $3z_{1/2}$ , the derived  $z_0$  is less than or equal to the RGB star  $z_0$  in each galaxy, as expected if the total stellar density is well characterized by a combination of the MS, AGB and RGB components. The fits presented here for these different stellar population components are in general not extremely sensitive to the range of  $z$  values used. Varying the lower limit of the fit between  $1.5-5z_{1/2}$  typically changed the AGB and RGB  $z_0$  values by less than 10%. The compact MS components were more dramatically affected because of the smaller number of stars at large scale heights.

From this analysis it appears that NGC 4631 has the “thickest” old component with an RGB scale height of  $\sim 1250$  pc, roughly 2.5 times larger than the MS and  $K_s$  band fits. We note that the fits for NGC 4631 were truncated at large negative disk heights to prevent the contamination of stars from companion galaxy NGC 4627. IC 5052 and NGC 4144 have similar ratios ( $\sim 2.5$ ) of RGB to MS scale heights, while NGC 4244 has the smallest ratio, with an RGB scale height only 1.7 times that of the MS stars.

There is also evidence for a modest flaring of the stellar components between the central and ‘-DISK’ pointings of NGC 55 and NGC 4631. The ‘-DISK’ fields are centered 4.8 and 6.1 scale lengths (see Table 2) from the center of the NGC 55 and NGC 4631 respectively. An increase in  $z_0$  values by a factor of 1.1 to 1.6 is seen for all three components in NGC 55 and for the AGB and RGB component in NGC 4631.

The profiles deviate from the fitted  $\text{sech}^2$  profile significantly near the midplane. This deviation is almost certainly due to dust, we model this effect in §4.4. At larger disk heights ( $>2-3$  kpc) there is also a slight overdensity in the RGB components of IC 5052, NGC 4144, NGC 4244 and NGC 5023. These overdensities hint at the possible presence of an even more broadly distributed old component. In three of these galaxies, the RGB fits had elevated  $\chi^2$  values relative to the MS and AGB fits. We estimate that these overdensities occur at a surface brightness  $\mu_{F606W} \gtrsim 28$  mag arcsec $^{-2}$  assuming a luminosity function similar to galactic globular clusters (Buonanno et al. 1994; Kravtsov et al. 1997). However, without better knowledge of the background level, it is not possible to verify the existence of this component.

The scale heights measured in the  $K_s$  band (Table 4) are closest to those measured for the MS and AGB components. Half of the galaxies have  $K_s$  band scale heights closer to the MS value and the other half closer to the AGB value. This suggests that the  $K_s$  band light in these galaxies is dominated by relatively young stellar populations, probably red supergiants and AGB stars (in agreement with the findings of Aoki et al. 1991). This result runs contrary to the common assumption that the NIR light primarily traces older stellar populations (e.g. Florido et al. 2001), and is significant in that NIR luminosity is often used as a proxy for stellar mass when comparing galaxies of different types and masses. However, we note that our  $K_s$  band scale heights are biased towards higher surface brightness populations due to the bright limiting isophote of the 2MASS data from which they are derived.

#### 4.2.2. Comparison to Previous Observations

The results above indicate that there is a systematic increase in the vertical scale heights of older stellar populations in our sample of low mass, late-type disks. Before investigating possible origins for these structural differences in §4.3 & §5, we now compare our measurements of scale heights to previous observations of the vertical structure of disks.

The most detailed constraints on the scale heights of different stellar populations come from the solar circle of the Milky Way. Studies have revealed a complicated disk structure, with a young and old thin disk embedded within a more extended thick disk. The young thin disk is the narrowest of the three, having a scale height of  $z_0 \sim 200$  pc, as traced by stars with bright absolute magnitudes ( $M_V \lesssim 3$ ) (Schmidt 1963). In contrast, the scale heights of the young main sequence stars in our sample are almost all significantly larger than the Milky Way value suggesting that the low mass galaxies in our sample form stars in a thicker layer than the Milky Way, consistent with Dalcanton et al. (2004). The resulting axial ratios for our samples' young star forming disks are also much thicker as well, with  $z_0/h_r = 1.8 - 6.3$  (see Table 4) for our sample galaxies, versus  $z_0/h_r \sim 15$  for the young thin disk of the Milky Way.

The division of the Milky Way's older stellar populations into a thin and thick disk was first introduced by Gilmore & Reid (1983) to explain a break in the number counts of F & G stars at  $\sim 1$  kpc. While the need for two old disk components was long debated, recent measurements of systematic  $\alpha$ -element enhancement in thick disk stars (most recently Gratton et al. 2003; Feltzing et al. 2003; Mishenina et al. 2004; Bensby et al. 2005) strongly suggest that the thick disk is indeed distinct from the old thin disk. Recent observations (Chen et al. 2001; Siegel et al. 2002) give a scale height for the old thin disk of  $z_0 \sim 600$  pc, similar to found in the original Gilmore & Reid (1983) study. These same studies suggest that the exponential scale height of the thick disk is  $h_z \sim 700$  pc (corresponding to  $z_0 \sim 1400$  pc, thinner than originally claimed). The Milky Way thick disk is therefore roughly twice the height of the old thin disk, and 7 times the height of the young thin disk.

Within our own sample, the scale height of the old RGB component is mostly intermediate between the Milky Way old thin disk and the thick disk. Our sample

galaxies have much lower masses and surface densities than the Milky Way, and, lacking any firm model that predicts how the properties of the old thin disk and the thick disk should vary with galaxy mass, we are hesitant to attribute the extraplanar population to either an old thin or a thick disk on the basis of the the surface brightness profiles alone. There are no dramatic inflection points in the RGB surface density profiles plotted in Figure 7 that would assist in a unique separation of old thin disk and thick disk stars, and the possible over-density of stars above 2-3 kpc may well be due to a stellar halo. Even if the RGB component is similar to the Milky Way thick disk, this lack of inflection is not unexpected. In the Milky Way, the inflection point in the surface density of F & G dwarves that marks the separation of the thin and thick disks is likely the result of two different populations of stars separated in age. The lack of similar inflection points in our RGB profiles can easily be explained if the RGB stars don't have as wide a range of ages as the Milky Way dwarves. We will show in §5 that the RGB stars in our galaxies may very well be dominated by a single-age population.

We do note, however, that the axial ratios of the RGB disks range between  $h_r/z_0 = 1.0 - 3.3$ , with a median of 1.8 (adopting the  $K_s$ -band radial scale length, and averaging the two independent measurements for NGC 55 and NGC 4631). For comparison, the axial ratios of the old thin and the thick disks of the Milky Way are 5.0 and 2.1, respectively (assuming  $h_r = 3$  kpc for both components). Thus, in terms of their *overall* structure, the RGB component we detect is significantly more round than the Milky Way's old thin disk, and is distributed more like the Milky Way thick disk. However, without additional information we cannot ascribe a common formation scenario to our observed RGB component and the Milky Way thick disk. We revisit this issue in the discussion (§6), after analyzing the disk heating and the vertical metallicity gradients of our sample galaxies.

Outside of the Milky Way, the most detailed information comes from studies of the vertical distribution of resolved stars in HST images, similar to the work we present in this paper. Tikhonov et al. (2005) and Tikhonov & Galazutdinova (2005) present evidence for extended components in six galaxies, which they qualitatively argue correspond to thick disks and halos. Of the galaxies that overlap our sample (NGC 55, NGC 4144, and NGC 4244), they include archival WFPC2 observations to reach greater disk heights in NGC 4244 and NGC 55 than spanned by our ACS images. In both cases they assume *a priori* that the RGB stars at lower disk heights trace a thick disk. For NGC 4244, Tikhonov & Galazutdinova (2005) show an exponential distribution of RGB stars between  $\sim 1$  and 3 kpc (their Figure 8) that appears to roughly match the scale height of the profile shown in Fig. 7. Beyond 3 kpc, they see a flattening in the number counts which they claim is a halo, but which may also be the background level. For NGC 55, Tikhonov et al. (2005) plot an exponential distribution of RGB stars between 2 and 7 kpc – i.e. at much greater disk heights than probed by our data. However, based on inspection of their Figure 12, the extended RGB component has a  $z_0$  value of  $\sim 2$  kpc, which is 2-3 times the width of the RGB component we fit. Although they assume this component is due to a thick disk based on its

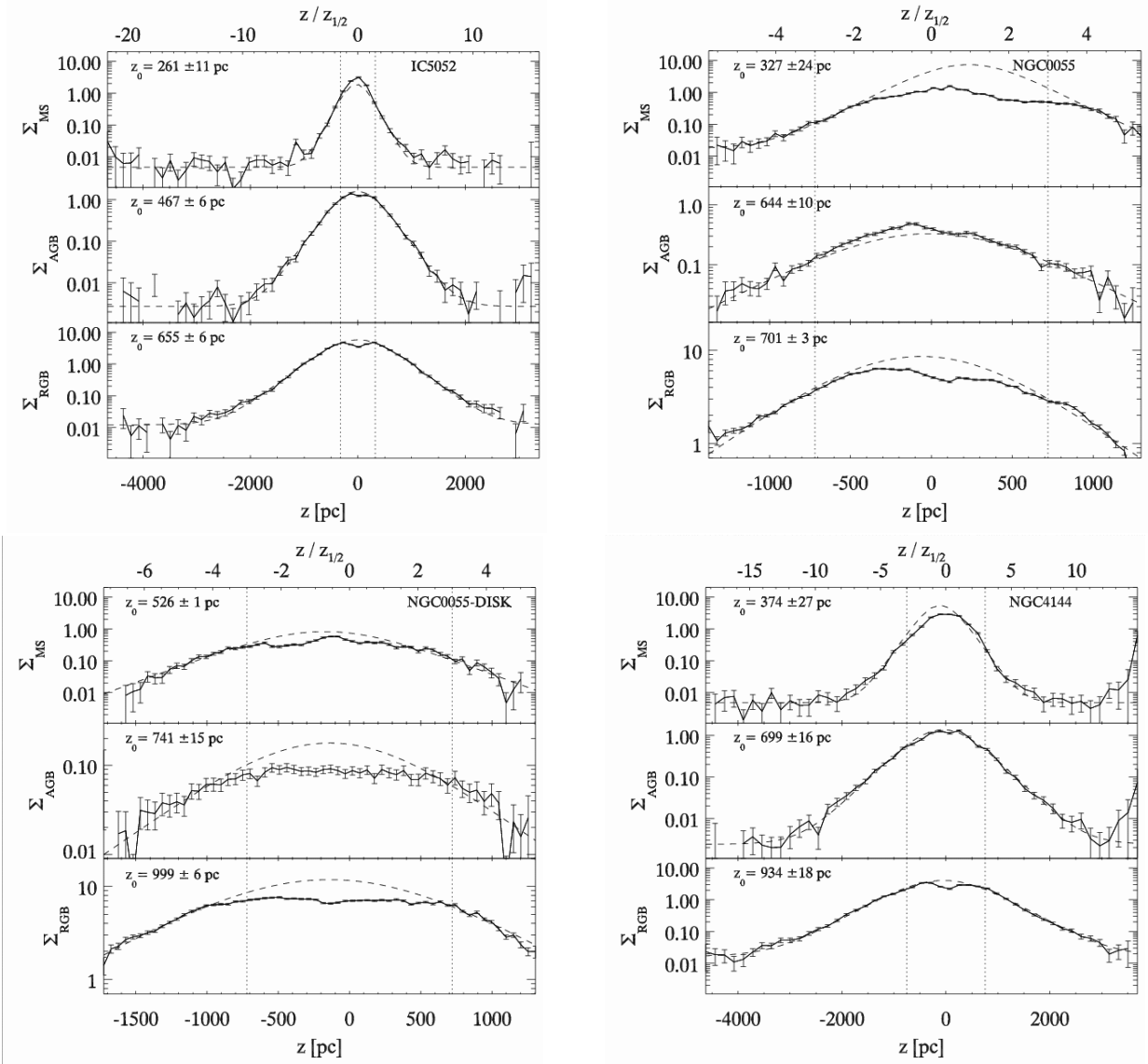


FIG. 7.— Model fits to the observed surface density distribution as a function of disk height in each galaxy for the MS (top), AGB (middle), and RGB (bottom). The dashed line shows the best fitting  $\text{sech}^2$  model excluding data with  $|z/z_{1/2}| < 3$  (as shown with the dotted lines) while the vertical dotted lines show the range of  $z$  values excluded from the fit. The number in the upper left corner gives the scale height of the best fitting  $\text{sech}^2$  function.

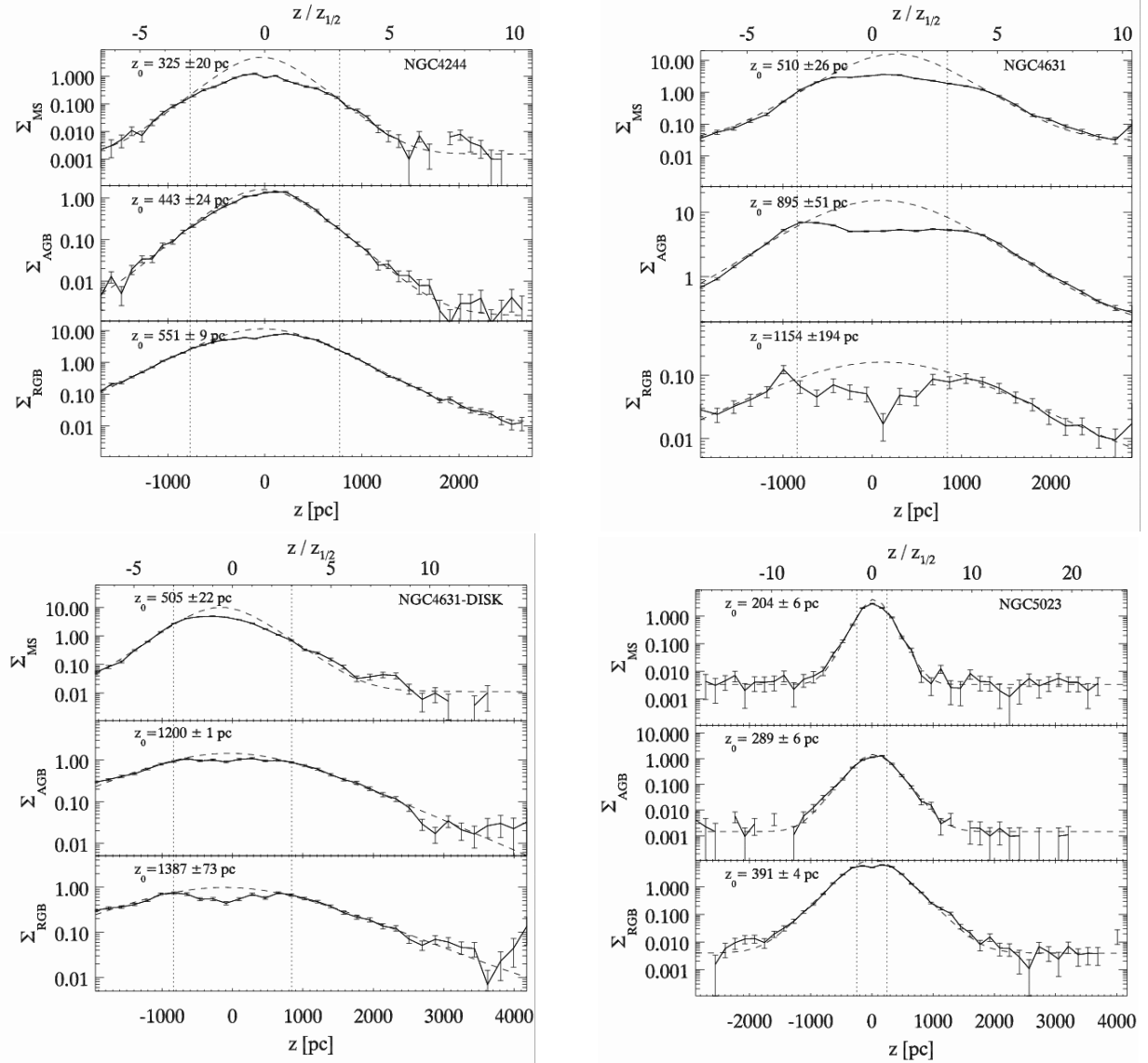
exponential surface density distribution, the axial ratio of this component would in fact be prolate ( $h_r/z_0 \sim 0.5$ ) and thus may be more analogous to the Milky Way's stellar halo<sup>3</sup>. The change in slope also implies a break in the RGB distribution in NGC 55 at around 2 kpc. By analogy, this may indicate that the marginal overdensities we are seeing at comparably large disk heights in our RGB profiles might be the signature of an additional broader halo component. Mould (2005) also finds the presence of old stars at large scale heights, and while these stars are automatically assumed to be a thick disk component, no detailed analysis of their spatial distribution is presented.

In addition to these recent studies of resolved stars, most previous studies of the vertical structure of

<sup>3</sup> Note, however, that NGC 55 is the least inclined galaxy in our sample, complicating the interpretation of its projected structural parameters.

disks have focused on detecting thick disks and stellar halos using unresolved surface brightness profiles of the galaxies (e.g. Pohlen et al. 2004; Fry et al. 1999; Dalcanton & Bernstein 2002; Neeser et al. 2002). Because we only detect stars at bright magnitudes, it is difficult to accurately convert our measured surface density of stars (Figure 2) to a surface brightness. However, assuming the outer parts of our galaxies have luminosity functions similar to Galactic globular clusters (Buonanno et al. 1994; Kravtsov et al. 1997), we estimate that we reach F606W surface brightnesses of  $\sim 28$  mag arcsec<sup>-2</sup>. This is comparable to the depth reached in deep ground-based observations.

Only one of our galaxies has been analyzed for vertically extended components using ground based data. Fry et al. (1999) present  $R$ -band surface photometry of NGC 4244 and find no evidence of a second thick disk

FIG. 7.— *continued*

component, based on the lack of an inflection point in the surface brightness distribution above the plane. They trace the vertical profile of NGC 4244 along the minor axis to  $\sim 2$  kpc at which point it falls below their surface brightness limit of  $27.5$  mag arcsec $^{-2}$ . We trace the RGB component out to nearly 3 kpc, and find a scale height that is similar to their fitted  $R$ -band scale height (assuming  $h_z = \frac{1}{2}z_0$ ). Their lack of an inflection in the surface brightness profile is consistent with the Tikhonov & Galazutdinova (2005) analysis to larger scale heights. This suggests that their fit was dominated by the old stars, and not a younger population. However, the lack of an inflection in the surface density distribution does not unambiguously rule out the presence of multiple components.

The ubiquity of thick disks in galaxies has previously been proposed by Dalcanton & Bernstein (2002) based on color-gradients in edge-on disk galaxies. Our observations confirm that the color-gradients (at least at the

low-mass end) are the result of true differences in stellar populations. However, whether these gradients have an analogous formation mechanism to the Milky Way thick disk is not clear.

One set of observations that reaches considerably deeper than these ground-based observations is presented by Zibetti et al. (2004), who used stacked Sloan images to show that halos are common in late-type, edge-on galaxies. Their composite galaxy has a significantly wider field of view and poorer resolution than our observations. They show that the best-fitting model to their data is a disk+halo model, with the disk component dominating out to roughly 10 exponential scale heights ( $\sim 10z_{1/2}$ ). Their limited resolution and combination of a heterogeneous sample of galaxies would likely prevent them from seeing the RGB components we see in our galaxies. However, the possible detection of the more extended RGB components detected in IC 5052, NGC 4144, and NGC 5023 may be halos similar to the Zibetti et al.

(2004) halo.

#### 4.3. Disk Heating

The increase in  $z_0$  seen in each galaxy between the MS, AGB and RGB populations (Fig. 7, Table 4) could result from a number of mechanisms, including vertical heating of a thin disk. Such a model would naturally produce the observed trend of older stellar populations having larger scale heights. In Figure 8 we plot the increase in scale height with mean stellar age for four fields that span the observed behaviour in our sample. We plot scale heights for the RGB and AGB, normalized by the MS scale heights, with the height of the symbols indicating the  $1\sigma$  uncertainties on  $z_0$ . Note that when interpreting our data in the context of disk heating models we are therefore implicitly assuming that the RGB and AGB stars were originally formed in a layer with a scale height comparable to that of the present day main sequence stars. We assign characteristic ages to the RGB and AGB using the MATCH synthetic CMD tests for a constant SFR (§4.1.1). However, because the galaxies' actual star formation histories may differ significantly from the constant SFR assumed in Figure 4, we cannot assign a single age to each stellar population. Instead, we use the resulting age distributions to identify the 25th, 50th (Median) and 75th percentile ages. The resulting age ranges are shown by the width of the individual boxes in Figure 8. However, note that the actual age of the population may lie entirely outside of the boxes, for example, if the RGB stars were all formed in a single burst 12 Gyr ago. Thus, when interpreting Figure 8, one has substantial allowance in assigning an age.

Overplotted on Figure 8 are dashed lines showing a range of power-law increases in the disk scale height  $z_0$  with time ( $z_0 \propto t^{-\beta}$ ). For an isothermal  $\text{sech}^2$  profile, the  $z_0$  values are related to the vertical velocity dispersion ( $\sigma_z$ ):

$$z_0 = \frac{\sigma_z^2}{2\pi G\Sigma} \quad (2)$$

where  $\Sigma$  is the surface density of the disk (Eq. 17 in van der Kruit 1988). Studies of disk heating traditionally use power laws in the velocity dispersion,  $\sigma_z \propto t^{-\alpha}$ , and thus  $\alpha = \beta/2$ . Figure 8 therefore demonstrates that the vertical velocity dispersion of our galaxies has increased no faster than  $\alpha = 0.15$ . More specifically, there are no characteristic ages that can be assigned to the AGB and RGB stars that yield heating rates greater than  $\alpha = 0.15$  (with the possible exception of the more massive, interacting galaxy NGC 4631), and thus this conclusion is robust even in light of our substantial age uncertainties.

In contrast, the disk heating that has been observed in the Milky Way is comparatively rapid. The age-velocity dispersion relation (AVR) for Milky Way disk stars suggests that the vertical velocity dispersion increases with time with values of  $\alpha$  ranging between 0.3 and 0.6 (e.g. Wielen 1977; Binney et al. 2000; Nordström et al. 2004, see summary in Table 1 of Hämmen & Flynn 2002). In contrast, our limit of  $\alpha \lesssim 0.15$  is significantly smaller than the Milky Way value. These data immediately suggest that any disk heating in our low mass galaxies has been far less effective than in the Milky Way. Moreover, if some fraction of the extraplanar RGB stars are not due

to disk heating, and are instead due to direct accretion or *in situ* formation at large scale heights, or if the RGB stars are weighted towards old ages (as we argue below in §5), then the actual rate of disk heating is even lower than suggested by Figure 8.

There are several reasons why disk heating is expected to be low for our sample galaxies. Within the Milky Way, the increase in vertical velocity dispersion with time is thought to be due to scattering by spiral arms (Barbanis & Woltjer 1967; Sellwood & Carlberg 1984; Carlberg & Sellwood 1985), by molecular clouds (Spitzer & Schwarzschild 1951), or both (Carlberg 1987; Jenkins & Binney 1990; Jenkins 1992; Shapiro et al. 2003, see also the review by Lacey 1991). However, our galaxies have sufficiently low masses and surface densities that they are unlikely to be globally gravitationally unstable (Dalcanton et al. 2004; Verde et al. 2002) and thus would not host strong spiral arms. Given that scattering by spiral arms seems to be the dominant heating mechanism in the Milky Way (e.g. most recently De Simone et al. 2004), the absence of spiral arms alone should cause a drastic drop in heating rate down to  $\alpha \sim 0.2 - 0.25$ , the expected value for heating by giant molecular clouds alone (e.g. Hämmen & Flynn 2002). Likewise, the absence of strong dust lanes in these systems and the results of §4.4 both indicate that the cold molecular ISM is in a thicker layer than in the Milky Way. This large scale height for the cold ISM, and the general lack of molecular gas in low mass galaxies (Young & Scoville 1991; Leroy et al. 2005) should therefore further suppress the efficiency of disk heating. Finally, the young stellar disks in our sample are apparently much thicker than in the Milky Way, which could reduce the efficiency of any heating mechanism (Freeman 1991). Shapiro et al. (2003) also argue for reduced disk heating in late-type galaxies based on the ratio of vertical to radial velocity dispersions. However, their rationale for the observed trend is opposite from what we conclude from our data.

As an aside, the low observed heating rates may provide strong constraints on cosmologically important sources of disk heating including late-time satellite accretion (Quinn et al. 1993), massive black holes (Lacey & Ostriker 1985), or halo substructure (e.g. Hämmen & Flynn 2002; Benson et al. 2004). However, the expected heating rates for such models have been calibrated for massive spiral disks, not the thicker, lower surface density galaxies studied here.

#### 4.4. Modelling Dust Effects on the Stellar Density Profiles

Before continuing to explore the origin of extraplanar stars, we briefly examine the vertical distribution of the dust layer. At first glance, interpretation of the stellar density profiles near the midplane in Figure 5 might be somewhat confusing. If the dips in surface density are due to dust, why does the dust appear to affect the RGB and AGB stars more than the MS stars? We suggest this may occur because the dust layer is opaque near the midplane and is distributed with a scale height greater than or equal to the MS population, but less than the AGB/RGB populations. The MS stars we are seeing would then lie entirely in front of an obscuring dust screen, while the AGB/RGB populations would have a

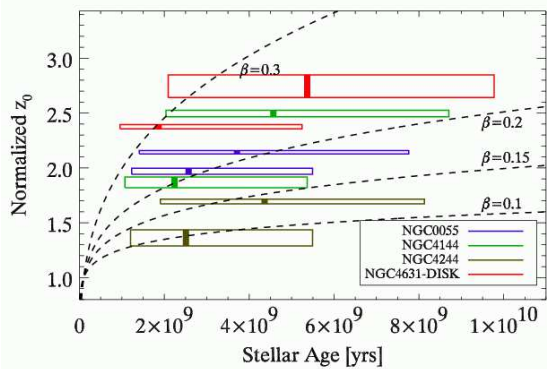


FIG. 8.— This figure shows the increase of scale height with time based on the stellar populations analysis described in §4.1-2. The AGB and RGB scale heights are shown for four galaxies spanning the range of  $z_0$ . Each scale height is shown with a box, color coded by galaxy. The box width represents the 25th, 50th, and 75th percentile age range of the AGB or RGB population (see Fig. 4) and the height represents the  $1\sigma$  errors in the determined  $z_0$  (Fig. 7). The  $z_0$  values were normalized by the  $z_0$  of the MS population. The dashed lines show power-laws of the form  $z_0 \propto t^{-\beta}$ . The RGB (upper) bar and AGB (lower) bar for any galaxy can be used to roughly constrain the disk heating rates. Because the precise star formation history of these components is not known, the width of the boxes is derived from a constant star formation rate model and thus represents the range of ages that contribute to the AGB and RGB population.

significant population at large disk heights above where the galaxy becomes optically thin. The dip in their numbers near the midplane is then explained because the optically thick dust layer obscures some fraction of the stars along the line of sight.

To test this explanation, we built a simple ‘toy model’ galaxy with MS, RGB and AGB populations distributed as  $\text{sech}^2$  profiles with the  $z_0$  as shown in Table 4. All components were given identical radial distributions with the  $K_s$  band exponential scale length. The dust component was assumed to also follow a  $\text{sech}^2$  profile with a variable scale height,  $z_{0,\text{dust}}$ , and a radial distribution identical to that of the stars. For simplicity we assumed that the dust has no effect at an optical depth less than one, but is completely obscuring at greater optical depths. Thus, along a line of sight, the dust is completely transparent to  $\tau = 1$ , and completely opaque beyond. For each vertical position we integrated the dust component along the line-of-sight until an optical depth of one was reached, which set the depth of the dust screen at that height. Stellar density profiles for the three separate populations were then created by totaling the number of stars in front of the dust screen at each height. We then normalized the stellar density profiles as in Figure 5.

Figure 9 shows the resulting model of NGC 4144 for three values of  $z_{0,\text{dust}}$  presented for comparison to the observations shown in Figure 5. In each case the amount of dust in the midplane is the same. The underlying values for  $z_0$  were adopted from Table 4 (374, 699, and 934 pc for the MS, AGB and RGB respectively). The left panel shows the results for a dust layer whose scale height is narrower than all three stellar components. For this case, there is a pronounced dip in the surface density profile of all three components. In the middle panel, the value of  $z_{0,\text{dust}}$  is between the  $z_0$  values for the MS and the AGB/RGB populations. In this case there is a dip

only in the AGB/RGB, because the height of the MS layer is entirely confined within the opaque dust layer, allowing only the unobscured stars on the near side of the galaxy to be detected. The right panel has a dust layer larger than the both the MS and AGB value and therefore a dip is seen only in the RGB component. The middle panel does a good job of qualitatively matching the observations for NGC 4144 in Figure 5.

Referring back to Figure 5, we can see that the main sequence profile lacks a dip near the midplane for most of the fields, while the RGB has a dip in all cases within 2-3  $z_{1/2}$ . This suggests that the dust in the galaxy is opaque below 2-3  $z_{1/2}$  and that it is distributed in a layer with thickness greater than or equal to the MS stars. Because the MS stars are already distributed in a thicker distribution than in the Milky Way, this result supports the Dalcanton et al. (2004) finding that galaxies with circular velocities below 120 km s $^{-1}$  have large dust scale heights and do not form thin dust lanes. All of the galaxies presented here except NGC 4631 are below this circular velocity limit (Table 1).

This model also suggests that although the depth to which we see in each galaxy is different at differing scale heights, it is the same for all the stellar populations at a single scale height. This validates the comparisons made in Fig. 6 between the ages of the stellar populations at different scale heights.

Although this model matches the gross characteristics of many of the profiles shown in Fig. 5, it fails to fully explain their details. Most notably, in NGC 55 and NGC 4244, the MS profiles are significantly lower than the best-fitting  $\text{sech}^2$  function, contradicting the idea that all the stars we are seeing lie in front of a screen. This is likely the result of our model’s lack of sophistication. Physically, it doesn’t take into account the possibility of flares or changing scale lengths as a function of stellar population. In addition, it treats dust extinction in a very simplistic fashion. A more sophisticated treatment of the dust (such as the one presented by Matthews & Wood 2001) is beyond the scope of this paper. The conclusions reached in this section should be considered tentative and will be tested in a later paper, in which we will present a more realistic dust model.

## 5. METALLICITY DISTRIBUTION FUNCTIONS

As has been shown previously (e.g. Da Costa & Armandroff 1990; Armandroff et al. 1993; Frayn & Gilmore 2002), the color of the red giant branch near its tip can be used to constrain the metallicity of old stellar populations. Although reddening due to dust will prevent an accurate measurement of the metallicity of stars near the midplane, we can determine a rough metallicity for stars above the midplane where the effect of dust and the contamination from AGB stars are small (as shown in Figure 6, middle panel).

Figure 10 shows a composite CMD of all high-latitude stars (above  $4z_{1/2}$ ) in IC 5052, NGC 55, NGC 55-DISK, NGC 4144, NGC 4244, and NGC 5023. This disk height limit was chosen (1) to be well above any of the dips associated with dust in Figure 5, (2) to dramatically reduce contamination by AGB and HeB stars that might interfere in the metallicity determination, and (3) to be where thick disk stars dominate in the Milky Way (Chen et al. 2001). Overlaid on the CMD are 10 Gyr old RGB

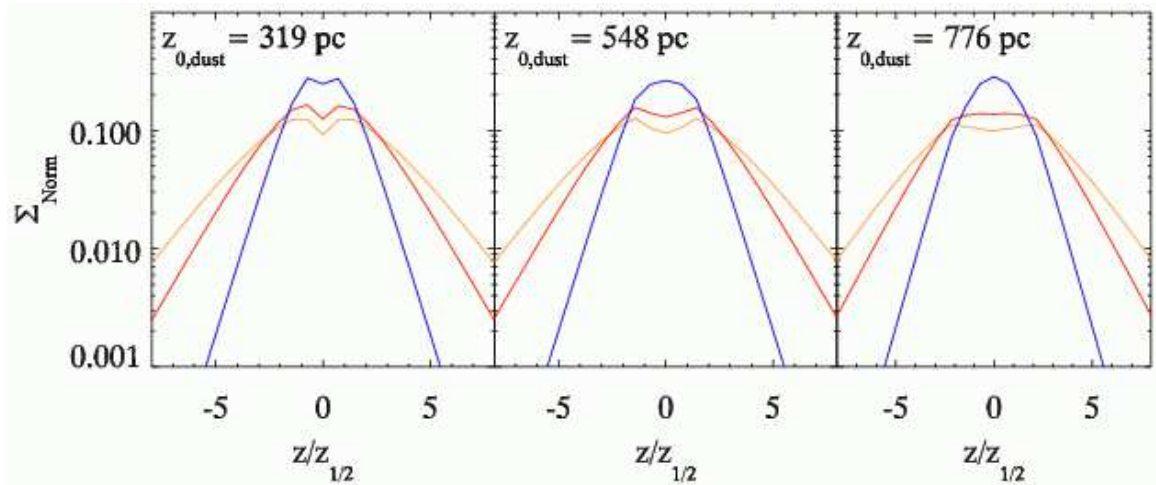


FIG. 9.— Toy models including the effects of dust on the stellar density profiles of NGC 4144. The three panels show different values of the dust scale height  $z_{0,\text{dust}}$ . The blue, red, and orange/yellow lines in each panel represent the MS, AGB, and RGB profiles respectively. Comparison to Figure 5 shows that the middle panel best matches the observations.

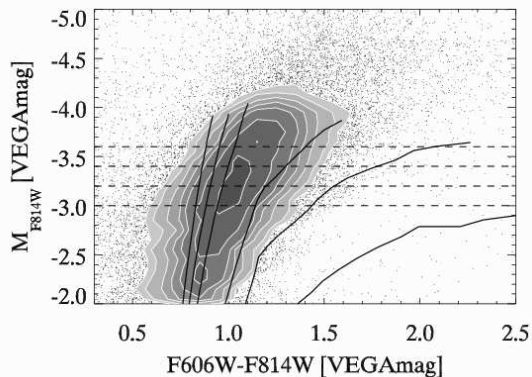


FIG. 10.— Composite CMD showing the red giant branches of IC 5052, NGC 55, NGC 55-DISK, NGC 4144, NGC 4244, and NGC 5023 at disk heights  $>4z_{1/2}$ . The absolute magnitude  $M_{F814W}$  was determined using the TRGB distance modulus in Table 1. Solid lines show 10 Gyr old Padova models for the RGB with  $[\text{Fe}/\text{H}]$  (from left to right) of -2.3, -1.7, -1.3, -0.7, -0.4, and 0.0. The peak of the stellar distributions fall between  $[\text{Fe}/\text{H}]$  of -1.3 and -0.7. Dashed lines indicate the three bins used to determine the metallicity distribution functions shown in Fig. 11.

isochrones (Girardi et al. 2000) at metallicities ranging from  $[\text{Fe}/\text{H}] = -2.3$  to 0.0, with higher metallicities being redder. Examination of Figure 10 shows that the peak of the distribution falls between the  $[\text{Fe}/\text{H}] = -1.3$  and -0.7 lines. Roughly 13% of the stars fall bluewards of the  $[\text{Fe}/\text{H}] = -2.3$  isochrone, probably due to a combination of photometric error and the presence of AGB stars. Very few are redder than the  $[\text{Fe}/\text{H}] = -0.4$  isochrone. Overall, Figure 10 indicates that most of the stars above  $4z_{1/2}$  are moderately metal-poor.

Improving on the metallicity determinations in Paper I, here we will derive metallicity distribution functions (MDFs) using untransformed magnitudes and Padova isochrones (Girardi et al. 2000). To determine metallicity distribution functions for individual galaxies we binned the stars in up to three independent 0.2 magnitude wide bins centered on  $M_{F814W}$  of -3.5, -3.3, and -

3.1. These are shown with dashed lines in Figure 10. The brightest bin was chosen to include stars as metal-rich as  $[\text{Fe}/\text{H}] = -0.4$ , which do not get brighter than  $M_{F814W}$  of -3.7. We considered only the magnitude bins that were above the 20% completeness cutoff for crowded regions (thus excluding the fainter bins in NGC 4144, see Figure 1). This cut eliminated NGC 4631 and NGC 4631-DISK from the analysis, because none of the bins fell above their 20% completeness limits. We corrected the colors and magnitudes of each star for foreground reddening, but made no correction for completeness, since the change in completeness across the color-range in question is similar to the error that would be introduced by that correction. We then determined the metallicity of each star by linearly interpolating between the 10 Gyr isochrones in each bin. Since some of the stars bluewards of the  $[\text{Fe}/\text{H}] = -2.3$  isochrone may be RGB stars scattered to bluer colors by photometric error, we attempted to include these stars in the MDFs. In each bin, stars bluer than the  $[\text{Fe}/\text{H}] = -2.3$  isochrone were given positive color shifts by multiplying a Gaussian random number by their error. This correction moved  $\gtrsim 50\%$  of these stars redwards of the  $[\text{Fe}/\text{H}] = -2.3$  isochrone, and resulted in a slight increase ( $\sim 0.01$  in the normalized units) in the MDF between a  $[\text{Fe}/\text{H}]$  of -1.3 and -2.3. Table 5 gives the resulting number of stars used in MDF determination, the median F606W-F814W error, and the peak and mean metallicities of the MDFs.

Figure 11 shows the resulting MDFs for each field. The shaded regions show the total range in the MDFs as derived in the different magnitude bins, and indicate that our results are consistent among the different magnitude ranges. In general, the MDFs peak at metallicities  $[\text{Fe}/\text{H}]$  of -0.7 to -1.1 as expected from Figure 10, and have a tail of stars to low metallicities.

Before analyzing the MDFs further, we note that there are several uncertainties in the detailed shapes of the metallicity distribution functions. First, they are based on isochrone models and not empirical data (as in Sarajedini & Van Duyne 2001). Second, the color errors on the metal-poor end (Table 5) translate into a

TABLE 5  
 METALLICITY DETERMINATIONS

Field	Paper I [Fe/H]	# of stars	$\sigma$ (F606W-F814W)	MDF Peak [Fe/H]	Mean [Fe/H]
IC 5052	-1.22	3770	0.21	-0.7	-0.9
NGC 55	-1.41	1068	0.09	-1.0	-1.0
NGC 55-DISK	-1.62	983	0.06	-1.1	-1.2
NGC 4144	-1.50	1773	0.19	-0.9	-1.0
NGC 4244	-1.45	1970	0.11	-0.9	-1.0
NGC 4631	-1.25				
NGC 4631-DISK	-1.54				
NGC 5023	-1.71	1119	0.22	-0.9	-1.0

NOTE. — The columns from left to right are: Field name, the metallicity estimated in Paper I, the number of stars used in the metallicity determination in this paper, the typical color error of those stars, the peak of the metallicity distribution function (from Fig. 11), and the mean metallicity.

large error in metallicity. We estimated the errors as a function of metallicity by inserting stars of a specific metallicity/color, giving them appropriate color errors, and then determining the spread in the resulting metallicity distribution. This procedure gave errors of 0.5-0.8 dex at  $[\text{Fe}/\text{H}] = -2.3$ . However, the shape of the distributions are much more believable on the metal-rich end where the isochrones are well separated, giving errors of less than 0.1 dex at  $[\text{Fe}/\text{H}] = -0.4$ . At the peak of the MDF ( $[\text{Fe}/\text{H}] \sim -0.9$ ), typical errors are 0.2 dex, suggesting that the peak metallicities derived here are fairly reliable.

Comparing the peak metallicity of the extraplanar stars to known Milky Way populations, Figure 11 indicates that the metallicities of the extraplanar stars are a factor of ten times too high to be analogs of the Milky Way’s stellar halo ( $[\text{Fe}/\text{H}] \sim -1.7$ , Wyse & Gilmore 1995). This result would not change even if all the stars bluewards of the  $[\text{Fe}/\text{H}] = -2.3$  isochrone are low metallicity RGB stars. We note however, that the low metallicity of the Milky Way halo may not be typical. The halo of Andromeda has been found to be much more metal-rich than in the Milky Way, with a peak  $[\text{Fe}/\text{H}] \sim -0.6$  (Holland et al. 1996; Brown et al. 2003), although there is difficulty ascribing these outer stars to a halo population *per se*, given M31’s complicated outer structure (Ferguson et al. 2002).

Of all the Milky Way components, we find that the peak metallicities are most consistent with those of the metallicity of the Milky Way thick disk, which has  $[\text{Fe}/\text{H}] \sim -0.8$  based on F/G dwarfs (Wyse & Gilmore 1995). The extraplanar stars studied here are somewhat more metal poor than the Milky Way’s thick disk (by up to 0.3 dex). However, this offset may not be surprising given the lower mass of our galaxy sample ( $V_c \sim 80 \text{ km s}^{-1}$  vs  $V_c \sim 220 \text{ km s}^{-1}$  for the Milky Way).

As in the Milky Way (Wyse & Gilmore 1995; Haywood 2001), the metallicities of the extraplanar stars appear to be more metal poor than the thin, young, main sequence population. Although dust prevents us from reliably measuring the metallicity of stars near the mid-plane, we can estimate their metallicity using the current gas phase metallicity. NGC 55, the only galaxy in our sample with a gas phase abundance measurement, has  $12 + \log(\text{O}/\text{H}) = 8.32$  at one disk scale length (Garnett

2002). This metallicity corresponds to  $[\text{Fe}/\text{H}] \sim -0.6$  (assuming  $[\text{Fe}/\text{O}] = 0$ ), which is 0.5 dex more metal rich than the extraplanar stars at a comparable radius. Other late-type disks with similar rotational velocities from the Garnett (2002) compilation have comparable gas-phase metallicities, suggesting that the offset in metallicity between the midplane and the extraplanar populations is likely to be systematic.

Although they do not explicitly examine stars as a function of scale height, studies of metallicities in other galaxies using methods similar to ours also find broad agreement with the presence of an extended  $[\text{Fe}/\text{H}] \sim -1$  population of RGB stars. The LMC (which has a mass similar to the galaxies in our sample) has a peak metallicity distribution of  $[\text{Fe}/\text{H}] \sim -0.6$  for RGB stars in the disk (Cole et al. 2000). Recent papers on the outer regions of M33 also find peak  $[\text{Fe}/\text{H}]$  values of -1.0 (Davidge 2003; Tiede et al. 2004). Furthermore, a recent paper by Davidge (2005), derives a  $[\text{Fe}/\text{H}]$  of roughly -1 for NGC 55 using near-IR photometry of resolved extraplanar stars, closely matching our peak metallicity in Figure 11. Our data and others therefore suggest the pervasive presence of a significant  $[\text{Fe}/\text{H}] \sim -1$  old population in late-type galaxies. If our association of this population with a thicker disk is generally true in other galaxies, then it presents an attractive solution to the “G-dwarf” problem seen in the Milky Way by providing the necessary prompt initial enrichment for stars in the thin disk (Truran & Cameron 1971).

Overplotted on Figure 11 as dashed lines are the expected metallicity distributions for closed-box “simple” chemical evolution models (Eq. 20 of Pagel 1997) scaled to the peaks of the MDFs. While the basic shape of these models are similar to our MDFs, there appears to be a deficit in some galaxies of stars at both low and high metallicities. A deficit at high metallicities is expected if star formation truncates before all the gas is consumed. Within the context of thick disk formation models, this truncation may occur if some of the gas reservoir that forms the extraplanar stars instead settles into the thin disk, if the extraplanar stars were heated from a previously thin but gas-rich disk, or if the extraplanar stars were directly accreted from merging satellites that suffered from tidal stripping or supernova blowout. The apparent deficit of stars at low metallicities may be another



manifestation of the widespread G-dwarf problem. Thus, while the existence of a substantial population of stars at  $[\text{Fe}/\text{H}] \sim -1$  may help to solve the G-dwarf problem in the thin disk, it may have simply pushed the problem into a new component. The solution to the extraplanar G-dwarf problem will likely lie among the suite of popular models previously explored for the thin disk (see Pagel 1997). However, some of the deficit of stars at low metallicities may also result from the photometric errors and methods used to construct the MDFs, as discussed above.

Finally, we note that the peaks of the metallicity distribution functions given in Table 5 are significantly more metal-rich than our previous determination presented in Paper I. Rather than using native F606W–F814W colors, these earlier measurements applied the metallicity-color relation of Lee et al. (1993) to the mean color of the giant branch transformed to the Johnson-Cousins filter system. These previous values, reproduced in Table 5, range from  $[\text{Fe}/\text{H}]$  of -1.2 to -1.7, versus -0.7 to -1.1 in the present work. We believe that in addition to the magnitude transformation, the difference in derived metallicity results in part from the difference in binning (in  $[\text{Fe}/\text{H}]$  vs. F606W–F814W), such that the mean color does not correspond to the peak metallicity. This offset can be seen in the 0.1-0.2 dex offset between the mean and peak metallicity in Table 5. Furthermore, the Paper I determination also included stars at somewhat lower disk heights, thereby increasing the number of AGB contaminants. We believe that the MDFs and their peak metallicity that we present here are more reliable than the estimate given in Paper I.

### 5.1. Vertical Metallicity & Color Gradients

Models for the origin of extraplanar stars (i.e. disk heating, direct accretion, etc.) predict different degrees of variation in the stellar metallicity with height above the plane. To investigate the vertical variation of metallicity with disk height  $z$  we have examined the median color of the RGB stars as a function of the height above the midplane. Figure 12 shows the median color of RGB stars between  $M_{\text{F814W}}$  of -3.2 and -3.6 and redwards of F606W–F814W=0.7, binned by the scale height of the galaxies. Data are plotted where errors in the median color are  $<0.05$  magnitudes. The hatched region at low disk heights shows where the effects of internal reddening may impact the colors of the stars. For the three fields with profiles extending beyond 2-3 kpc we bin the RGB stars at large disk heights in a single bin to reach adequate signal-to-noise in our measurement of the median color, plotted as diamonds in Figure 12. We note that these are the same stars that comprise the possible extended components discussed in §4.2.

Figure 12 demonstrates three main points. First, the color gradients in the galaxies are relatively small, indicating that the stars have nearly uniform metallicity with increasing distance above the plane, particularly at scale heights above the region potentially affected by dust. However, we note that the stars at very large radii (shown with diamonds) do tend towards bluer colors, possibly indicating the presence of a more metal-poor population at  $z \gtrsim 10z_{1/2}$  (2-3 kpc). Second, the color gradients show no systematic trends, and are equally likely to be rising or falling. Finally, all the galaxies have very similar RGB

colors (as demonstrated already in Figure 11).

Our metallicity gradient results are consistent with previous observations of these and other low-mass spiral galaxies (Davidge 2005; Tikhonov et al. 2005; Mould 2005). Mould (2005) used HST archival data to study the vertical properties of disks in four low-luminosity ( $M_V \sim -16$ ) edge-on galaxies comparable to those studied here. Using AGB, RGB, and red supergiant stars over a large range of magnitudes ( $-8.5 \lesssim M_I \lesssim -1.5$ ), he calculates the mean colors up to 2 kpc from the plane. His main results are that there are slight or no color gradients as a function of disk height and that the metallicities of the stars at disk heights between 400 and 2000 pc are between -0.8 and -1.0 in all four galaxies, in excellent agreement with what we find here. Tikhonov et al. (2005) also state that any metallicity gradient in NGC 55 is very small, in agreement with our observed lack of color-gradients in Figure 12. Recent simulations of thick disks by Brook et al. (2005) also show a lack of any metallicity gradient with disk height.

The lack of strong metallicity gradients can be explained in a number of ways. Mould (2005) suggests the lack of metallicity gradients rules out dissipative and simple accretion models for thick disk formation, and favors a model in which thick disks form during interactions. We note that the lack of metallicity gradient may also be enhanced by an “age-bias” in the metallicity measurements. The mass of stars on the RGB changes from  $\sim 2 M_\odot$  at an age of 1 Gyr to  $<1 M_\odot$  at 10 Gyr. Given the steepness of the IMF in this mass range, the RGB age distribution will be weighted towards older ages, and therefore to a more uniform metallicity. However, based on the constant star formation rate models in §4.1, it still appears that the RGB stars could span a wide range of ages, even in the presence of the expected age-bias. Therefore, the simplest interpretation of the lack of gradients in our data is that many of the RGB stars at disk heights above  $4z_{1/2}$  ( $\sim 1$  kpc) formed at a similar time and thus have comparable enrichment histories, eliminating any metallicity gradient. This scenario could be explained either by a sudden heating of the disk by interaction, or by accretion of gas-rich satellites which resulted in the formation of a thick component. N-body simulations have shown that early merging and accretion events can produce thick disks with old ages (Abadi et al. 2003; Brook et al. 2004; Brook et al. 2005).

## 6. DISCUSSION & CONCLUSIONS

The work presented here has identified a number of main observational results:

- In low mass, late-type galaxies the thickness of a stellar population increases systematically with the age of the stars being studied. This behavior has been seen not just in all six of the galaxies studied here, but in all other HST studies of edge-on late-type galaxies, and in the Milky Way as well. The larger scale heights of older stellar populations is therefore likely to be a generic property of galaxy disks.
- All of the studied galaxies show a clear intermediate age (1 – 5 Gyr old) population whose scale height is intermediate between that of the young main sequence stars and the older red giants.

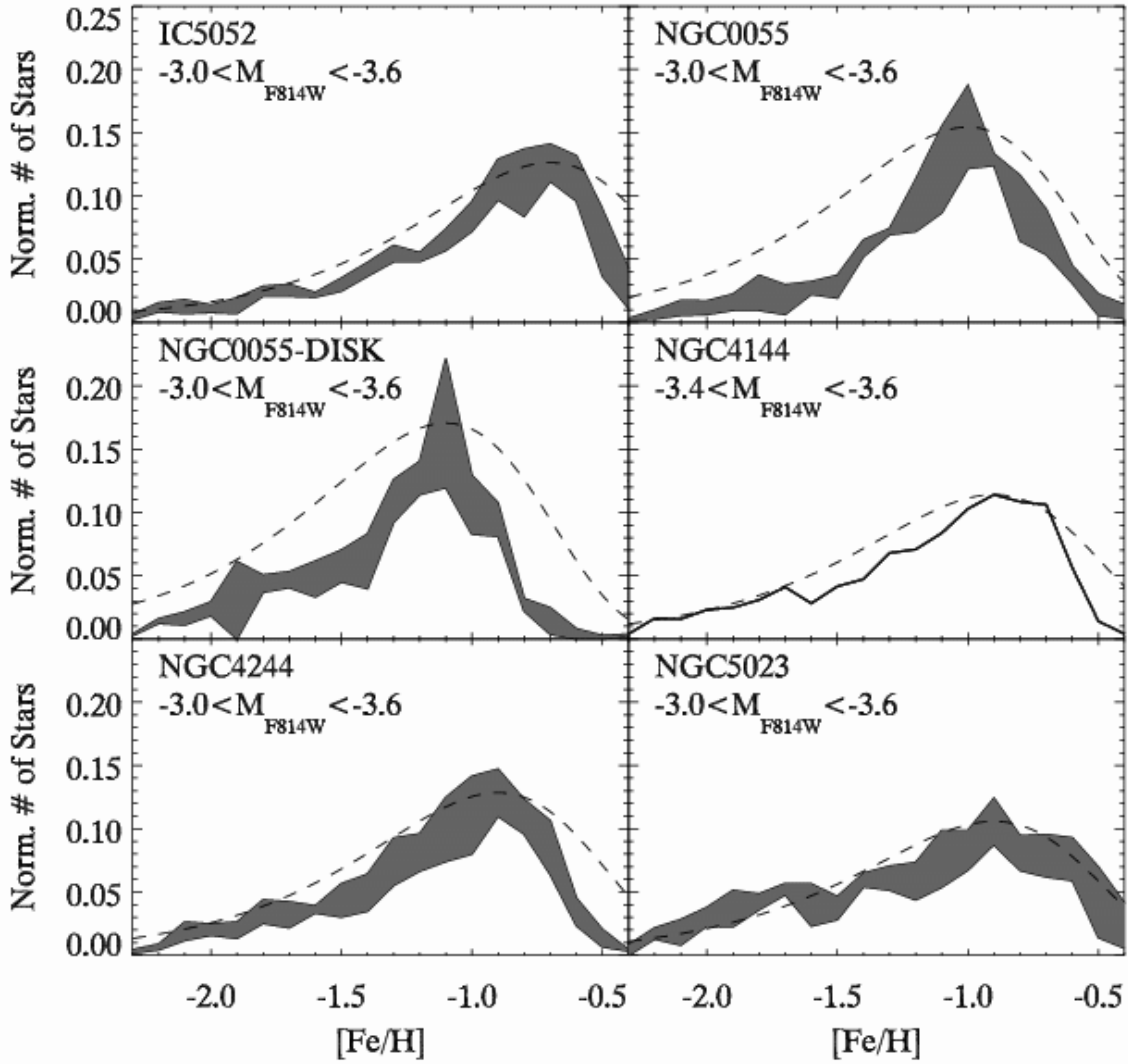


FIG. 11.— Metallicity distribution functions for stars at disk heights  $>4z_{1/2}$ . Gray regions indicate the range of values obtained in different absolute magnitude bins. The bins used for this determination are 0.2 magnitudes wide and are shown in Fig. 10. Only bins above the magnitude limits in Table 3 were used. Dashed lines indicate closed-box chemical evolution models scaled to the peak of the MDF.

- The metallicity of the dominant old stellar population has  $[\text{Fe}/\text{H}] \sim -1$ , but shows little or no gradient between  $3z_{1/2}$  and  $10z_{1/2}$  above the plane. Above this height ( $> 2 - 3$  kpc), there are tentative indications of decreasing metallicities, which may be associated with slight overdensities in the RGB surface density at similar distances above the midplane.
- In the low mass galaxies studied here ( $V_c \sim 70 - 130$  km sec $^{-1}$ ), the young stellar population is systematically thicker than in the MW, and has a vertical scale height comparable to the thickness of the dust layer. This suggests that the cold ISM has a larger scale height in low mass galaxies, consistent with the lack of dust lanes observed in such systems (Dalcanton et al. 2004).
- The young and intermediate-age stellar populations dominate the integrated *near-infrared* light of late-type low mass galaxies.

We now interpret these observational facts in the context of disk formation models. First, taken at face value, the old RGB component's  $\sim 3:1$  axial ratio and  $[\text{Fe}/\text{H}] \sim -1$  metallicity suggest a close correspondence with the Milky Way's thick disk. However, each of our galaxies' scale heights steadily increase from the young main sequence to the intermediate age AGB and the older RGB. The uniformity of this trend strongly suggests that our disks are not simply the superposition of two components (i.e. a thick and thin disk). Instead, the data require a more complex model incorporating some disk heating to explain the systematically larger scale height of the intermediate-age population. The necessary disk heating would also have affected any older population, and thus must make some contribution to the thicker population of RGB stars. The required amount of disk heating is much smaller than is seen in the Milky Way (§4.3), and could likely be provided by molecular clouds or minor mergers. The latter scenario is slightly favored by the large variations in the apparent change of disk scale height with

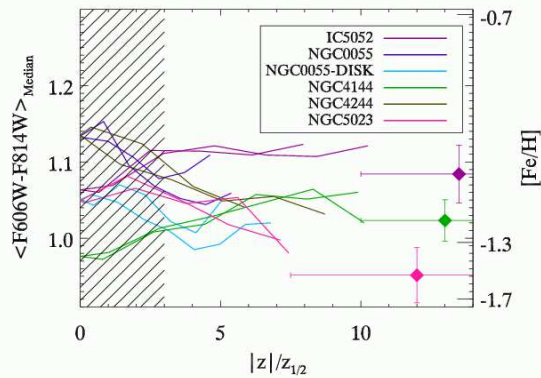


FIG. 12.— The median RGB color as a function of disk height in each galaxy. This includes stars with  $F606W-F814W$  redder than 0.7 and  $M_{F814W}$  between  $-3.2$  and  $-3.6$ . The error on all plotted data is  $<0.05$  magnitudes. The diamonds indicate the median color of all stars at large disk heights and is plotted only for the three galaxies with significant numbers of stars at large scale heights. The hatched area indicates the heights at which internal reddening may affect the stellar colors. The right axis shows the mean RGB color of Padua isochrones (Girardi 2004) at three different metallicities.

time (Figures 6 & 8). Heating through satellite accretion and interaction could naturally produce these stochastic variations. However, numerical simulations of heating in diffuse low mass disks would be required to definitively constrain any of the above scenarios and to assess how significant a contribution heating may have made to the thicker RGB component.

While the above argument strongly suggests that disk heating must play some role in the production of the extraplanar stars, the lack of a metallicity gradient in RGB stars at moderate disk heights (500 – 2000 pc, as shown here and in Mould 2005) suggests that steady disk heating cannot entirely explain the thickest component of old RGB stars. If the past star formation rate has been constant, then there is a significant overlap between the stellar ages of the AGB and RGB regions of the color-magnitude diagram (Figure 4). A significant fraction of the RGB stars should therefore have smaller scale heights, younger ages, and enriched metallicities, and would thus produce a steady increase in metallicity towards the midplane for all but the most contrived scenarios. The most attractive explanation for the lack of metallicity gradient is that instead of a constant star formation rate, the majority of RGB stars at all scale heights must have formed early and with a well-mixed metallicity distribution. Such a population would dwarf any subsequent population of enriched RGB stars with lower scale heights. While steady dynamical heating could push this ancient population to larger scale heights, it could not simultaneously account for recent dynamical observations of counter-rotating disks at these disk

heights in comparable galaxies (Yoachim & Dalcanton 2005). Taken together, these observations are better explained by scenarios involving the formation of a thick disk of stars in merger events (as in Abadi et al. 2003; Brook et al. 2004; Brook et al. 2005). Overall, our results require that some disk heating occurs at intermediate ages (to puff up the AGB component), but that events at earlier times (interactions or mergers) created a majority of the RGB stars over a short timescale.

Finally, we present tenuous evidence for an extended old component seen only at disk heights  $> 2-3$  kpc. At large scale heights we see marginal overdensities of stars in the RGB profiles of Fig. 7. There also seems to be a reduction in the metallicity of RGB stars at this height (Fig. 12). In one of our galaxies, Tikhonov et al. (2005) finds strong evidence for a very extended component of RGB stars extending from  $\sim 2-7$  kpc. While this component appears to have an exponential distribution, its  $z_0$  value of  $\sim 2$  kpc (compared to a radial scale length of  $\sim 1$  kpc) strongly suggests it is not a disk. These extended components are detected at about the same height where the halo becomes prominent in the stacked Sloan images of Zibetti et al. (2004). However, based on our observations, we are unable to assess the properties or frequency of these components.

The present-day structure of galaxy disks results from a complex mixing of effects and a full explanation requires detailed knowledge of the star formation history, merging events, and disk heating. Studies like the one presented here help to disentangle these effects and determine their relative importance as function of galaxy type and mass. This study also shows the promise that HST observations of resolved stars have for enabling the detailed analysis of low surface brightness stellar components in galaxies outside the Local Group. A comparison of our data with N-body simulations of low mass disk galaxies would assist in constraining disk heating and merging scenarios. Unfortunately, current simulations of disk galaxy formation have focused on massive galaxies like the Milky Way (Abadi et al. 2003; Brook et al. 2004; Brook et al. 2005). Also, deeper observations that fully resolve the red and blue horizontal branches would greatly improve constraints on the star formation histories of these galaxies and improve our understanding of their structure.

Acknowledgements: The authors would like to thank Andrew Dolphin and Antonio Aparicio for their help in generating synthetic CMDs, Leo Girardi for supplying us with isochrones, our anonymous referee for their thoughtful suggestions, and Peter Yoachim, Andrew West, and Kevin Covey for helpful discussions. This work was supported by HST-GO-09765, the Sloan foundation, and NSF Grant CAREER AST-0238683.

#### REFERENCES

- Abadi, M. G., Navarro, J. F., Steinmetz, M., & Eke, V. R. 2003, *ApJ*, 597, 21  
Aoki, T. E., Hiromoto, N., Takami, H., & Okamura, S. 1991, *PASJ*, 43, 755  
Aparicio, A., & Gallart, C. 2004, *AJ*, 128, 1465  
Armandroff, T. E., Da Costa, G. S., Caldwell, N., & Seitzer, P. 1993, *AJ*, 106, 986  
Barbanis, B., & Woltjer, L. 1967, *ApJ*, 150, 461  
Becker, R., Mebold, U., Reif, K., & van Woerden, H. 1988, *A&A*, 203, 21  
Bekki, K., & Chiba, M. 2001, *ApJ*, 558, 666  
Bensby, T., Feltzing, S., Lundstrom, I., & Ilyin, I. 2005, *Astron. Astrophys.*, 433, 185  
Benson, A. J., Lacey, C. G., Frenk, C. S., Baugh, C. M., & Cole, S. 2004, *MNRAS*, 351, 1215

- Bertelli, G., Bressan, A., Chiosi, C., Fagotto, F., & Nasi, E. 1994, *A&AS*, 106, 275
- Binney, J., Dehnen, W., & Bertelli, G. 2000, *MNRAS*, 318, 658
- Brook, C. B., Gibson, B. K., Martel, H., & Kawata, D. 2005
- Brook, C. B., Kawata, D., Gibson, B. K., & Freeman, K. C. 2004, *ApJ*, 612, 894
- Brown, T. M., Ferguson, H. C., Smith, E., Kimble, R. A., Sweigart, A. V., Renzini, A., Rich, R. M., & Vandenberg, D. A. 2003, *ApJ*, 592, L17
- Buonanno, R., Corsi, C. E., Buzzoni, A., Cacciari, C., Ferraro, F. R., & Fusi Pecci, F. 1994, *A&A*, 290, 69
- Burstein, D. 1979, *ApJ*, 234, 829
- Carlberg, R. G. 1987, *ApJ*, 322, 59
- Carlberg, R. G., & Sellwood, J. A. 1985, *ApJ*, 292, 79
- Chen, B., Stoughton, C., Smith, J. A., Uomoto, A., Pier, J. R., Yanny, B., Ivezić, Z., York, D. G., Anderson, J. E., Annis, J., Brinkmann, J., Csabai, I., Fukugita, M., Hindsley, R., Lupton, R., Munn, J. A., & the SDSS Collaboration. 2001, *ApJ*, 553, 184
- Cole, A. A., Smecker-Hane, T. A., & Gallagher, J. S. 2000, *AJ*, 120, 1808
- Da Costa, G. S., & Armandroff, T. E. 1990, *AJ*, 100, 162
- Dalcanton, J. J., & Bernstein, R. A. 2002, *AJ*, 124, 1328
- Dalcanton, J. J., Yoachim, P., & Bernstein, R. A. 2004, *ApJ*, 608, 189
- Davidge, T. 2005, *astro-ph/0501173*
- Davidge, T. J. 2003, *AJ*, 125, 3046
- de Grijs, R., & Peletier, R. F. 1997, *A&A*, 320, L21
- de Grijs, R., & van der Kruit, P. C. 1996, *A&AS*, 117, 19
- De Simone, R., Wu, X., & Tremaine, S. 2004, *MNRAS*, 350, 627
- Dolphin, A. E. 2002, *MNRAS*, 332, 91
- Eggen, O. J., Lynden-Bell, D., & Sandage, A. R. 1962, *ApJ*, 136, 748
- Feltzing, S., Bensby, T., & Lundström, I. 2003, *A&A*, 397, L1
- Ferguson, A. M. N., Irwin, M. J., Ibata, R. A., Lewis, G. F., & Tanvir, N. R. 2002, *AJ*, 124, 1452
- Florido, E., Battaner, E., Guijarro, A., Garzón, F., & Jiménez-Vicente, J. 2001, *A&A*, 378, 82
- Frayn, C. M., & Gilmore, G. F. 2002, *MNRAS*, 337, 445
- Freeman, K., & Bland-Hawthorn, J. 2002, *ARA&A*, 40, 487
- Freeman, K. C. 1991, in *Dynamics of Disc Galaxies, Proceedings of Varberg Conference*, ed. B. Sundelius, 15–+
- Fry, A. M., Morrison, H. L., Harding, P., & Boroson, T. A. 1999, *AJ*, 118, 1209
- Garnett, D. R. 2002, *ApJ*, 581, 1019
- Gilmore, G. 1984, *MNRAS*, 207, 223
- Gilmore, G., & Reid, N. 1983, *MNRAS*, 202, 1025
- Gilmore, G., Wyse, R. F. G., & Norris, J. E. 2002, *ApJ*, 574, L39
- Girardi, L. 2004, private communication
- Girardi, L., Bressan, A., Bertelli, G., & Chiosi, C. 2000, *A&AS*, 141, 371
- Gnedin, O. Y. 2003, *ApJ*, 589, 752
- Gratton, R. G., Carretta, E., Claudi, R., Lucatello, S., & Barbieri, M. 2003, *A&A*, 404, 187
- Hänninen, J., & Flynn, C. 2002, *MNRAS*, 337, 731
- Haywood, M. 2001, *MNRAS*, 325, 1365
- Holland, S., Fahlman, G. G., & Richer, H. B. 1996, *AJ*, 112, 1035
- Hummel, E., & Dettmar, R.-J. 1990, *A&A*, 236, 33
- Hummel, E., Dettmar, R.-J., & Wielebinski, R. 1986, *A&A*, 166, 97
- Jenkins, A. 1992, *MNRAS*, 257, 620
- Jenkins, A., & Binney, J. 1990, *MNRAS*, 245, 305
- Kravtsov, V., Ipatov, A., Samus, N., Smirnov, O., Alcaïno, G., Liller, W., & Alvarado, F. 1997, *A&AS*, 125, 1
- Kroupa, P. 2002, *MNRAS*, 330, 707
- Kroupa, P., Tout, C. A., & Gilmore, G. 1993, *MNRAS*, 262, 545
- López-Corredoira, M., Cabrera-Lavers, A., Garzón, F., & Hammersley, P. L. 2002, *A&A*, 394, 883
- Lacey, C. G. 1991, in *Dynamics of Disc Galaxies, Proceedings of Varberg Conference*, ed. B. Sundelius, 257–+
- Lacey, C. G., & Ostriker, J. P. 1985, *ApJ*, 299, 633
- Lee, M. G., Freedman, W. L., & Madore, B. F. 1993, *ApJ*, 417, 553
- Leroy, A., Bolatto, A. D., Simon, J. D., & Blitz, L. 2005
- Marigo, P. 2001, *A&A*, 370, 194
- Martin, M. C. 1998, *A&AS*, 131, 77
- Matthews, L. D., & Wood, K. 2001, *ApJ*, 548, 150
- Mendez, R. A., & van Altena, W. F. 1998, *A&A*, 330, 910
- Mishenina, T. V., Soubiran, C., Kovtyukh, V. V., & Korotin, S. A. 2004, *A&A*, 418, 551
- Mould, J. 2005, *AJ*, 129, 698
- Narayan, C. A., & Jog, C. J. 2002, *A&A*, 390, L35
- Neuser, M. J., Sackett, P. D., De Marchi, G., & Paresce, F. 2002, *A&A*, 383, 472
- Ng, Y. K., Bertelli, G., Chiosi, C., & Bressan, A. 1996, *A&A*, 310, 771
- Nordström, B., Mayor, M., Andersen, J., Holmberg, J., Pont, F., Jørgensen, B. R., Olsen, E. H., Udry, S., & Mowlavi, N. 2004, *A&A*, 418, 989
- Ojha, D. K. 2001, *MNRAS*, 322, 426
- Olling, R. P. 1996, *AJ*, 112, 457
- Pagel, B. E. J. 1997, *Nucleosynthesis and chemical evolution of galaxies (Nucleosynthesis and chemical evolution of galaxies /B. E. J. Pagel. Cambridge : Cambridge University Press, 1997. ISBN 0521550610)*
- Paturel, G., Theureau, G., Bottinelli, L., Gouguenheim, L., Coudreau-Durand, N., Hallet, N., & Petit, C. 2003, *A&A*, 412, 57
- Paturel, G., Vauglin, I., Andernach, H., Garnier, R., Marthinet, M.-C., Petit, C., di Nella, H., Bottinelli, L., Gouguenheim, L., & Durand, N. 1995, *LEDA: The Lyon-Meudon Extragalactic Database (ASSL Vol. 203: Information On-Line Data in Astronomy)*, 115–126
- Pohlen, M., Balcells, M., Lütticke, R., & Dettmar, R.-J. 2004, *A&A*, 422, 465
- Pohlen, M., Dettmar, R.-J., Lütticke, R., & Schwarzkopf, U. 2000, *A&AS*, 144, 405
- Quinn, P. J., Hernquist, L., & Fullagar, D. P. 1993, *ApJ*, 403, 74
- Sarajedini, A., & Van Duyne, J. 2001, *AJ*, 122, 2444
- Schmidt, M. 1963, *ApJ*, 137, 758
- Sellwood, J. A., & Carlberg, R. G. 1984, *ApJ*, 282, 61
- Seth, A. C., Dalcanton, J. J., & de Jong, R. S. 2005, *AJ*, 129, 1331
- Shapiro, K. L., Gerssen, J., & van der Marel, R. P. 2003, *AJ*, 126, 2707
- Siegel, M. H., Majewski, S. R., Reid, I. N., & Thompson, I. B. 2002, *ApJ*, 578, 151
- Spitzer, L. J., & Schwarzschild, M. 1951, *ApJ*, 114, 385
- Tiede, G. P., Sarajedini, A., & Barker, M. K. 2004, *AJ*, 128, 224
- Tikhonov, N. A., & Galazutdinova, O. A. 2005
- Tikhonov, N. A., Galazutdinova, O. A., & Drozdovsky, I. O. 2005, *A&A*, 431, 127
- Truran, J. W., & Cameron, A. G. W. 1971, *Ap&SS*, 14, 179
- Tsikoudi, V. 1979, *ApJ*, 234, 842
- van der Kruit, P. C. 1988, *A&A*, 192, 117
- van der Kruit, P. C., & Searle, L. 1981, *A&A*, 95, 105
- Verde, L., Oh, S. P., & Jimenez, R. 2002, *MNRAS*, 336, 541
- Wielen, R. 1977, *A&A*, 60, 263
- Wyse, R. F. G., & Gilmore, G. 1995, *AJ*, 110, 2771
- Yoachim, P., & Dalcanton, J. J. 2005
- Young, J. S., & Scoville, N. Z. 1991, *ARA&A*, 29, 581
- Zibetti, S., White, S. D. M., & Brinkmann, J. 2004, *MNRAS*, 347, 556